2013

Antenna Designs for Wireless Medical Implants.

Conor P. Conran
IEEE, cpconran@gmail.com

Antenna Designs for Wireless Medical Implants

by

Conor Conran

This Report is submitted in partial fulfilment of the requirements of the Masters of Science Degree in Electronic and Communications Engineering (DT085) of the Dublin Institute of Technology

September 10th, 2013

Supervisor: Prof. Max Ammann
Antenna and High Frequency Research Centre
Dublin Institute of Technology

Declaration

I certify that this thesis which I now submit for examination for the award of a Master of Science is entirely my own work and that it has not been taken from the work of others, save and to the extent that such work has been cited and acknowledged within the text of my work.

This thesis was prepared according to the regulations for postgraduates of the Dublin Institute of Technology and has not been submitted in whole or in part for an award in any other Institute or University.

The work reported on in this thesis conforms to the principles and requirements of the Institute's guidelines for ethics in research.

The Institute has permission to keep, to lend or to copy this thesis in whole or in part, on the condition that any such use of the material of the thesis be duly acknowledged.

Dublin, 10. September 2011

_____

Conor Conran

Acknowledgements

I wish to thank Prof. Max Ammann and Dr. Matthias John of the Antenna and High Frequency Research Centre, Dublin Institute of Technology, for their time, advice and assistance in this research project.

I would also like to thank my father, Tom Conran, who inspired a love of radio technology from my earliest years. This work is dedicated to him, to my loving wife Inara and to our daughter Mia, who's now taking her first wobbly steps on life's learning journey.

Project Brief

Supervisor: Prof. Max Ammann, Antenna and High Frequency Research Centre.

Project Title: Antenna Designs for Wireless Medical Implants.

This project is suited for 1 student.

Tools: The following equipment was used during design and prototype production:

- Windows Workstation running CST Microwave Studio® simulation software.
- LPKF Protomat C60 CNC Milling Machine.
- VNWA3E Vector Network Analyser for empirical prototype refinement.

The following equipment was used during validation testing:

- Rohde and Swartz ZVA Vector Network Analyser.
- Rohde and Swartz FSP Spectrum Analyser.
- Rohde and Swartz SMC Signal Generator.

Project Type: Software modelling and hardware design.

Project Area: Radio frequency design, antenna prototype development and performance evaluation.

Project Synopsis:

The aim of this project was to research, develop and test antenna designs for wireless medical implants.

Phase 1 was to research academic and industry publications on the factors that affect antennas implanted inside the human body and to devise a suitable method to test them.

Phase 2 was to develop and simulate the performance of suitable antenna designs in vivo using an appropriate software tool.

Phase 3 was to produce prototype antennas and evaluate their performance.

Abstract

Active medical implants are devices that are surgically implanted inside the body. They have been developed to treat a wide range of ailments and many require some form of communications link with the outside world for diagnostics and maintenance.

Radio links promise a wide range of benefits over low frequency inductive coupling. However, body tissue is a challenging environment for both the device and the radio signal that it transmits. Innovation in medical technology is creating a demand for higher bandwidth and resilient implant links, and this in turn is driving the development of implantable antennas.

Many factors constrain antenna design choices. These include low signal power levels, minimal space availability and the effect that tissue characteristics have on the antenna. Most body tissues are highly dissipative and antennas must be specifically designed for a high dielectric environment.

A review of spectrum band availability indicates that the 401 – 406 MHz and 2.4 GHz bands are most suitable for implants. Multiband antennas were explored in the research, but the design priority focussed on 401 – 406 MHz.

Custom antenna designs were simulated in software and prototypes were later produced and tested in a range of different materials that closely imitate body tissue. These tests revealed a discrepancy in the software simulations. It affected all the prototypes, causing them to resonate at circa 150 MHz higher than the expected frequency.

The simulation software's transient domain solver was eventually identified as a likely cause of the frequency offset, but in the interim the antenna designs were progressed using empirical methods. The frequency domain solver has been found to predict the resonant frequencies of dielectrically loaded implant antennas with better accuracy than the time domain solver.

Two final designs were developed. Validation tests confirmed a good return loss of 10 to 20 dB in a replicated implant environment. The designs are meander line variants of an inverted-L antenna.

The design process, test results and detailed specifications are set out hereafter.

Table of Content

List of Figures

List of Tables

1. Introduction to Wireless Medical Implants

An active medical implant is an electronic device surgically implanted inside a human body or an animal. Implants have been developed to treat a diverse range of medical conditions, including pacemakers for cardiovascular disorders, cochlear implants for the hearing impaired and automated implantable medicine pumps to assist with conditions requiring frequent delivery of intravenous drugs.

Most implants require a communications link with the outside world in order to monitor the patient's condition and to facilitate periodic device reprogramming. Ongoing maintenance is also required, such as monitoring the condition of the device's internal battery. Once it has been implanted, the device is not removed again for maintenance or battery replacement unless absolutely necessary [9], as to do so requires the patient to undergo further surgery.

Communications with an *in vivo* implant requires a wireless communication link, as wired links are undesirable from the perspective of the patient's comfort and the risk of infection [14]. Historically this used low frequency inductive coupling between a coil inside the implant, and an external inductive probe.

The key limitations of inductive coupling are that it provides a relatively low bandwidth communications channel of circa 30 kbps, and it can only communicate over short distances of circa 10 cm [17] [23]. It also requires an external probe to be placed directly on the patient's skin for reliable communication, often requiring the assistance of a trained medical professional [2].

An alternative to inductive coupling is to use an electromagnetic radio signal. This provides more flexibility to patients and medical staff, allowing communications over longer distances and with faster data rates. Patients can also be remotely monitored using an intermediate wireless device in the home, reducing unnecessary visits to healthcare clinics. Recent innovations in medical diagnostic tools require wideband communication links which are beyond the capability of the traditional inductive coupling approach [15] [16].

Implant radio links require compact and efficient antennas that fit either inside or around the device's case. The design of such antennas is complex. The human body is a challenging environment which attenuates electromagnetic signals rapidly and reduces both the efficiency and bandwidth [1] of antennas that are designed to operate in free space.

2. Review of Implant Technology

This section discusses innovation in implant technology, the antenna requirements in this field and the technical challenges that must be overcome by the designer.

2.1 Innovations in Implant Technology that Influence the Development of Antennas

Wireless endoscopes are an example of the kind of medical applications that influence the development of implantable antennas. Diagnosing patients with digestive system ailments traditionally involved inserting wired endoscopes into the digestive tract, so that the affected area can be observed. This is an uncomfortable procedure for a patient to undergo. There is also a risk of damaging the delicate lining of the digestive tract, as well as the fact that the central six meters of the small intestine cannot be reached using a wired endoscope [22].

Pill-sized endoscope capsules can now deliver detailed images of the entire digestive system without risking injury or discomfort to the patient.

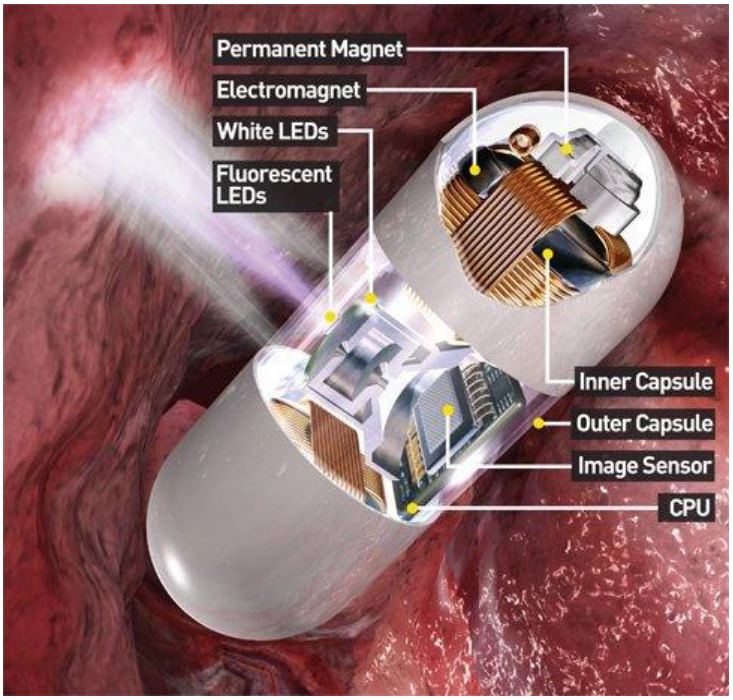

Figure 1: Wireless endoscope capsule (Source: Medi-Mation).

The images may be stored in onboard memory and viewed after the capsule is retrieved, however real-time viewing requires a wireless communications link. Diagnostic imaging requires high resolution cameras which produce circa 100 Mbps of data [8]. It is possible to compress this data, but the associated processing electronics place extra demands on the limited battery capacity and space available inside the 300 mm^3 capsule [22].

It is difficult to transmit 100 Mbps of data within the narrow bands that telecoms regulators have allocated to implants (e.g. 401 - 406 MHz), so research in this area is focusing on Ultra Wideband technology (UWB) [22].

UWB provides a high bandwidth communications link by transmitting rapid pulses that occupy bandwidths greater than 500 MHz. If high fidelity wideband antennas are used, these pulses can be radiated directly from the antenna, without requiring RF carriers or associated carrier modulation. This reduces the complexity, size and power consumption of the transmitter, but extremely wideband antennas are necessary to avoid distorting the pulses [22].

UWB is also useful for low data rate implant applications. It can reduce the time needed to transfer data, further extending the device's battery life [9]. It can also extend the communications range through processing gain[1]. The performance advantage provided by processing gain allows communication over longer distances, providing patients with more freedom of movement.

In addition to its communications benefits, UWB can also help to pinpoint the exact location of the implant within the body (and any tissue it's observing) by measuring time-of-flight of the radiated pulses [22].

2.2 Implant Antenna Design Challenges

Power supply and antenna space limitations are key implant antenna design considerations.

Implants are typically powered by small internal batteries and surgery is needed in order to replace them. There are alternative methods of supplying power, but they have limitations in terms of convenience for the user and the maximum power they can provide to the implant. Examples include "bio-fuel cells" which generate power by harnessing a controlled reaction between the dissolved oxygen and glucose that are present in the body's interstitial fluid. Bio-fuel cells are limited to very low power applications that consume less than 8 μW of power [6]. Another alternative is to supply power from a strong signal source located outside the body. An antenna or coil inside the implant receives a fraction of this energy, and it is used to power the device. A single implant antenna can be dual-purpose, i.e. receiving both the power and communication signals [13]. However, external power is impractical for permanent implant operation, as it restricts patient mobility and it becomes increasingly inefficient at higher frequencies [12].

An efficient antenna will extend the limited battery life, as it reduces the transmitter power needed for reliable communication. It is desirable to design an efficient and compact antenna; however these two factors are in conflict. Radiation resistance is the mechanism by which antennas dissipate RF energy as electromagnetic radiation. Compact antennas operating at low frequencies are inherently inefficient, as their

[1] Processing gain is a coding technique that improves a spread spectrum signal's immunity to noise. The improvement is proportional to the ratio of the un-spread information bit rate to the spread signal's bit rate [24].

radiation resistance is low and their reactance is high [24]. Efficiency can be increased by antenna design techniques and or lumped components to cancel reactance and match dissimilar impedances, but these approaches increase antenna loss. Using high frequencies to increase the efficiency of electrically small antennas is also impractical, as it incurs greater signal attenuation in body tissues which typically have high dielectric losses[2] [9].

The limited power available in implants means that the transmitter output power cannot be increased to compensate for antenna inefficiency or tissue attenuation.

Figure 2 below shows a plot of typical tissue attenuation in the 402 - 405 MHz band.

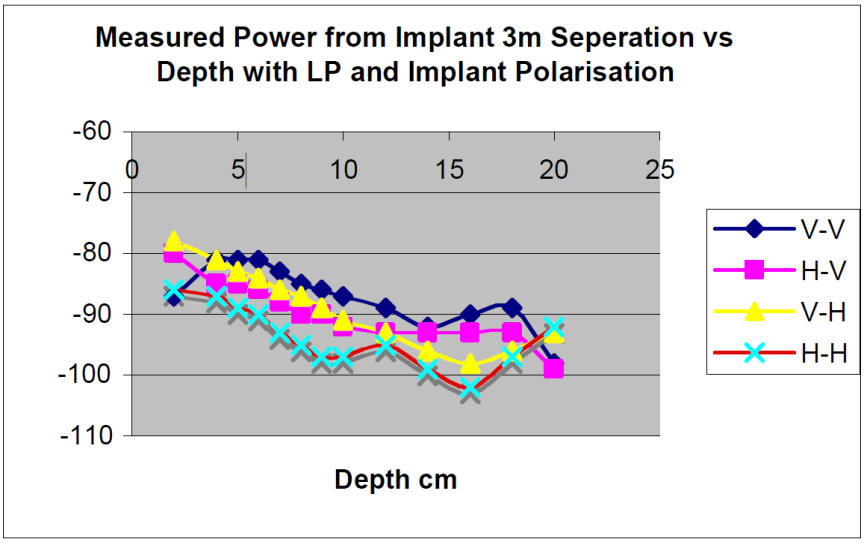

Figure 2: The measured propagation loss for a 403 MHz signal [9].

Propagation loss (dB) is shown on the Y-axis. The X-axis shows the results for a transmitting antenna located at various depths (cm) within the body. The receiving antenna is located 3 meters away from the body. There are four plots showing the results for vertical polarisation (V) and horizontal (H) polarisation in both the co-polar and cross-polar conditions.

Antennas that are designed to operate in free space typically suffer poor impedance matching when they are surrounded by dissipative body tissue [1] as the high dielectric constant of the tissue reduces the resonant frequency of the antenna.

[2] At radio frequencies (RF) the dielectric loss, or "dissipation", is caused by dipole polarisation of molecules within body tissues. Dipole polarisation is where opposing ends of the molecule have a net charge with respect to each other. An RF field interacts with the dipole polarised molecules, imparting motion to them. The resulting molecule vibration is dissipated energy in the form of heat. The dielectric properties of a material are described by its complex dielectric permittivity, which has a real *("non-lossy")* element and an imaginary *("lossy")* element. The ratio between the real and imaginary element, and hence how lossy the material is to an RF field, is referred to as its "*loss tangent*". The loss tangent of a material may vary with the frequency of the field. It can also vary with the temperature or moisture content of the material, or with variation in applied pressure. A material may be "*isotropic*", in that it has a constant loss tangent irrespective of the orientation of an RF field. Alternatively, a material may be "*anisotropic*", exhibiting a variable loss tangent depending on the field's orientation [27]. Muscle tissue is an example of the latter.

Impedance matching to tissue is complicated by variations in tissue characteristics. The dielectric and permittivity properties of tissue change from organ to organ and often also vary over time [1] [4]. For example, the characteristics of tissue may change depending on the individual's current level of hydration or as food transits through a nearby region of the digestive system.

Dissipative tissue also reduces antenna bandwidth [1]. If not mitigated this negates some benefits of UWB.

The proximity of other implants in the vicinity of the antenna can increase attenuation and even the position of the patient's limbs can increase propagation loss in the transmission path [11].

Non-deterministic sources of loss (such as tissue variation and limb position) must be mitigated by an appropriate fade margin in the link budget or the communications link with the implant becomes less reliable. Providing an adequate fade margin places greater demands on antenna efficiency.

The choice of antenna shrouding material is also an important design consideration. An antenna that is in direct contact with body tissue occupies less space than an antenna surrounded by a shroud of non-dissipative insulation material, but it results in higher loss due to tissue absorption [3]. Bio-compatible insulation avoids adverse tissue reaction and improves impedance matching [1] [20] [21]. The use of a shroud material with a high dielectric constant, low conductivity and low loss tangent can further reduce losses in dissipative body tissue, as it concentrates the electric near field components closer to the antenna, keeping them out of the surrounding dissipative tissue.

If the dielectric constant of the insulation material is between 40 and 50, similar to body tissue, then wideband antenna matching can be improved. Polyether-ether-ketone (PEEK) titanium-oxide and glycerine are considered to be suitable materials with a high dielectric constant and low permittivity [1].

3. Radio Spectrum Availability for Wireless Medical Implants

This section concentrates on the European and United States regulatory environments and identifies suitable frequencies for implant antenna designs.

The frequency of operation is a fundamental design consideration for any antenna. The choice of frequency band is constrained by spectrum allocations that are decided by regulatory organisations. These organisations decide how different frequencies are used at the national, regional and global levels. Frequency bands are often harmonised for a common use across many countries for the benefit of users and manufacturers.

Radio spectrum allocations and their associated regulatory regimes differ greatly between Europe and the United States. However there are a number of spectrum bands common to both regions which have been identified for use by exempted wireless devices, including wireless medical implants.

In Europe and the United States there are two possible approaches to operating wireless medical implant devices in a licence exempt environment (i.e. without requiring a licence to transmit). These options are:

- to operate in spectrum specifically identified for medical implant devices; or
- to operate in spectrum identified for exempt use more generally, where implants would share the spectrum with other applications and users.

3.1 Spectrum Availability in Europe

In Europe both options are possible under the Short Range Devices (SRD) regime which exempts certain categories of wireless devices. SRDs, as implied by their name, are devices intended to communicate over distances of a few meters up to several hundred meters. They are permitted to operate within specific frequency bands on the basis that they may not cause interference to other users and they may not claim protection from interference arising from other users. SRDs often share the same spectrum as licensed users and critical safety of life services. This is permitted on the basis that SRDs radiate low power levels and they must also incorporate specified mitigation[3] measures so that they coexist with other spectrum users.

The SRD bands and conditions of use are listed in ERC Recommendation 70-03[4]. This is a living document and is regularly updated by CEPT ECC[5] to reflect changes in its spectrum policy. Within the SRD framework, implant devices could operate in bands identified for:

[3] Such mitigation measures include limitations on transmission duty cycle or protocols such as "listen-before-talk".
[4] This document is available at http://www.erodocdb.dk/Docs/doc98/official/pdf/Rec7003e.PDF
[5] The Electronic Communications Committee (ECC) is the CEPT body with responsibility for radiocommunications and telecommunications matters. The ECC webpage is: http://www.cept.org/ecc

"Active Medical Implants and Their Associated Peripherals". Under this option, implant devices could operate in a limited number of bands, but with the benefit of a relatively predictable interference environment. Medical devices only have to coexist with the primary users of the bands and do not suffer interference from other exempted devices. A full list of these bands is presented in Appendix 2.

"Non-Specific Short Range Devices". Under this option, implants could operate in a wider selection of frequency bands, but they would share these bands with other licence exempt equipment, such as Bluetooth enabled devices, RFID tags and 802.11 computer networks (WiFi). It is likely that implant devices operating in these bands would suffer interference from many sources. Moreover, as new exempted devices and applications are continually being introduced into the market, their cumulative activity is likely to increase the level of interference within these bands in the future. For this reason the non-specific SRD bands cannot provide a predictable interference environment over the longer term.

Given the long service life of many implants (typically 10 to 15 years), uncertainty over the long-term reliability of their wireless links is undesirable. This is particularly the case for devices that treat critical medical conditions. A full list of the bands for non-specific SRDs is presented in Appendix 2.

3.2 Spectrum Availability in the United States

In the United States there is no direct equivalent to the European SRD regime, but the Federal Communications Commission[6] (FCC) has identified a number of bands between 401 MHz and 457 MHz for what is referred to as the "Medical Device Radio Communications Service" or "MedRadio" (These bands include the 401 – 406 MHz band). The full list of MedRadio bands available in the United States is provided in Appendix 2.

Devices may also operate on a non-interference and non-protected basis in the Industrial, Scientific and Medical (ISM) bands[7]. The ISM bands cannot provide implant users with a long-term predictable interference environment for the same reasons that apply to non-specific SRD use in Europe. Appendix 2 provides a list of the permitted ISM bands in the United States.

3.3 Candidate Bands for the Proposed Development of Medical Implant Antennas

A number of practical factors constrain the selection of candidate frequency bands for consideration. These factors include:

[6] The Federal Communications Commission is the Government body tasked with regulating the use of the radio spectrum resource in the United States. See: http://www.fcc.gov for details.
[7] This is subject to mitigation requirements similar to those applying to European SRD spectrum use.

- Antennas optimised for bands that are available in both Europe and the United States will yield greater economic and social benefits for users and device manufacturers.

- Skin penetration loss and the propagation loss through body tissue will have a significant impact at higher frequencies. It is therefore likely that bands in spectrum significantly above 2.5 GHz should not be considered (for example 5.8 GHz, 24 GHz and above).

With regard to these factors, there are three bands that are suitable candidates for antenna research. These are analysed in turn below with reference to the regulatory regime that applies in Europe.

The first proposed band for study is **401 - 406 MHz**. This band is 5 MHz wide in total and medical implants may use channels of up to 300 kHz within the centre 3 MHz of the band (i.e. 402 – 405 MHz). More restrictive conditions apply closer to the band edges. All 5 MHz of the band is shared with meteorological aids[8] but the likelihood of suffering interference is low due to relatively sparse use of the band by the Meteorological Service. This band is available for active medical implants in both Europe and the United States. The band plan presented in Figure 3 outlines the conditions of use in Europe.

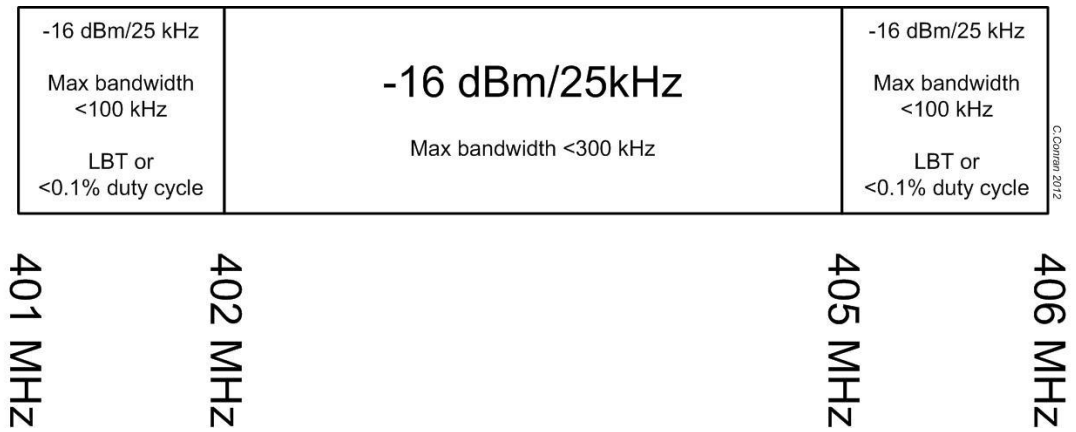

Figure 3: 401 - 406 MHz band plan and conditions of use in Europe.

The second proposed band for study is **2.4 - 2.5 GHz**. This spectrum encompasses both[9] the 2400 – 2483.5 MHz non-specific SRD band and the 2483.5 – 2500 MHz band which wireless medical implants are also permitted to use. The majority of the band is shared with non-specific Short Range Devices and so the likelihood of suffering interference in spectrum below 2483.5 MHz is high. This band is available

[8] According to ITU Recommendation ITU-R SA.1346 on compatibility between mmeteorological aids and implant devices, the 401 - 406 MHz band is used for weather data gathering devices such as radiosondes, rocketsondes and dropsondes and the risk of interference to implant devices is expected to be low.

[9] The full 100 MHz of this band can be used by medical implants that employ Listen Before Talk (LBT) and Adaptive Frequency Agility (AFA) mitigation. A transmit duty cycle of 10% or less is also required.

in both Europe and the United States. The band plan presented in Figure 4 outlines the conditions of use in Europe:

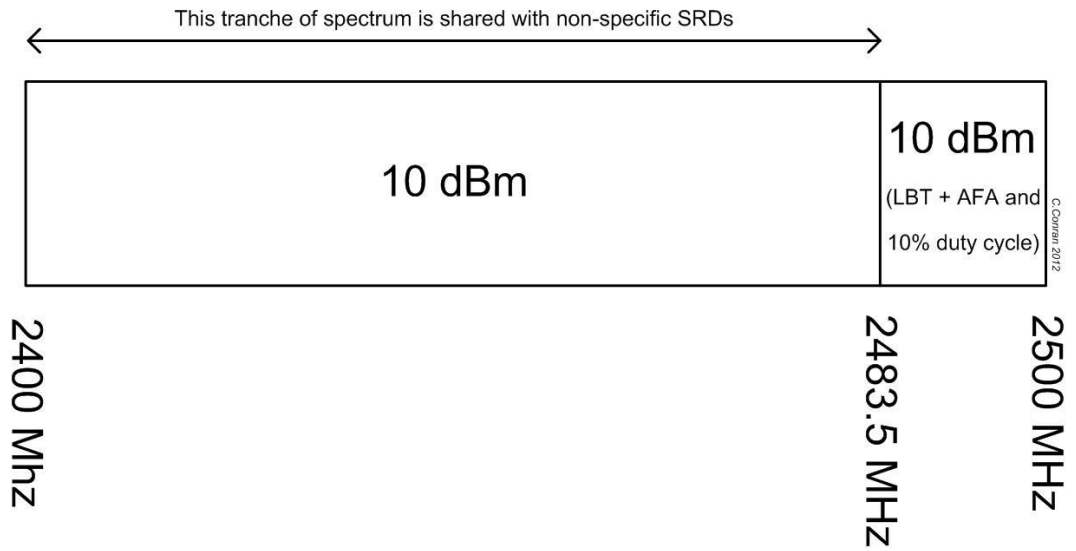

Figure 4: 2.4 - 2.5 GHz band plan and conditions of use in Europe.

A third band for consideration is **863 - 870 MHz**, however this band is only available in Europe[10]. The band is shared with non-specific Short Range Devices and the likelihood of suffering interference is high. A possible alternative band in the United States market is the 902 – 928 MHz ISM band, as it is close to 870 MHz. A single antenna may be able to cover both of these bands. The 863 - 870 MHz band plan presented in Figure 5 outlines the conditions of use in Europe:

Figure 5: 863 - 870 MHz band plan and conditions of use in Europe.

[10] This band is 7 MHz wide. It can be used in Europe by wireless medical implants employing Direct Sequence Spread Spectrum (DSSS) with Listen Before Talk (LBT) and Adaptive Frequency Agility (AFA) mitigation techniques.

3.4 Conclusions on Antenna Design Frequency

Antenna design should focus on the following bands in order of priority;

- The highest priority is the 401 – 406 MHz band. This band is harmonised for implant use in both Europe and the US. It also affords implanted devices the greatest protection against interference as it is not available to other exempted devices.

- Of lesser priority is the 2.4 - 2.5 GHz band. This band is available for exempt use in most parts of the world. However, implants would not be protected from interference caused by other exempted devices and high power users[11].

- The lowest priority is a combination of the 863 – 870 MHz and/or 915 MHz bands. Considered together, these bands could accommodate users in both Europe (863 MHz) and the US (915 MHz) but the bandwidth available is low and implanted devices are not protected from interference.

It is desirable to design a multi-band antenna that can be used in both the 401 – 406 MHz and 2.4 - 2.5 GHz bands. This is because some implant devices[12] use a 2.4 GHz wakeup signal to initiate a communications session in the 401 – 406 MHz band. This allows the device to switch off much of its receiver circuitry when it is not required, helping to conserve battery power.

[11] In parts of the 2.4 GHz band, SRD devices such as Bluetooth and WiFi adapters can transmit at power levels of 100 mW. In many countries the Radio Amateur Service is also permitted to transmit at power levels of up to 400 Watts (26dBW) EIRP.

[12] An example of an implant processor chip with an integrated 2.4 GHz "wake up" receiver is the Zarlink ZL70102. Further information is available at http://ulp.zarlink.com/zarlink/hs/82_ZL70102.htm

4. Research Methodology

This section provides a brief description of the procedure used to design, build and test the prototype antennas that were developed for the bands discussed in the preceding section.

4.1 Computer Simulation and Prototyping

The antenna designs were modelled using CST Microwave Studio® simulation software (CST). Early antenna models assumed a free space environment in order to reduce the computation time required for computer simulation [20]. Later designs were simulated in body tissue (phantom).

The early prototype antennas were handmade for proof of concept. A Computer Numerical Control (CNC) milling machine was used to print later prototypes on FR4 substrate[13].

The antenna prototypes were wrapped in meat or immersed in artificial liquid-based phantoms. The literature suggested a liquid phantom[14] consisting of sugar, salt and Hydroxyethylcellulose (HEC) diluted in deionised water. [3] [4] [25].

4.2 Prototype Validation Testing

In order to verify that the prototypes met the performance predicted in the computer simulations, the frequency response and return loss (S_{11}) of the antennas was measured using a Rohde and Swartz ZVA Vector Network Analyser (VNA).

Revised prototypes were milled and retested in an iterative process to develop an understanding of the effect of immersion in body tissue.

4.3 Calibration of Test Equipment

The prototypes were fully immersed in the phantom during testing in order to accurately simulate an *in vivo* environment. RF connectors were not mounted directly on the prototype antennas, as phantom material ingress into the connector or test cable could distort the test results. To prevent this, rigid coaxial "pigtails" were soldered directly onto the prototype antennas so that the test equipment's connectors and cables did not come into contact with the phantom. However, this complicated the test equipment calibration procedure.

In order to accurately calibrate a VNA for phase and impedance measurements, the reference plane must be set at the location of the antenna's feed point. If the reference plane is not correctly set, then cable effects (propagation delay and attenuation) add uncertainty to impedance and S_{11} measurement results. As the prototypes used pigtail

[13] The FR4 substrate used for the prototypes was 0.4 mm thick with double-sided 35 µm thick copper surfaces.

[14] The resulting mixture had a dielectric constant of 49, relative permeability of 1 and conductivity of 0.6 S/m which closely simulates the average properties of human body tissue [3] [4] [25].

cables instead of connectors, it was not possible to connect precision terminations[15] directly at the feed point. A 15 cm pigtail could distort measurements if it is ignored during calibration.

Two calibration pigtails were prepared so that the VNA's reference plane could be set precisely at the antenna feed point. These were sections of coax with open and shorted cable ends. They were identical to the pigtails on the antenna prototypes and they were used as a proxy for open and short terminations during the calibration procedure.

4.4 Ferrite Chokes on Feeders

In order to test a prototype antenna it is necessary to connect it to a VNA. RF current may flow from an antenna's ground plane, along the outside of the coaxial cable in common mode. It can also conduct electrical noise to the antenna from mains wiring, via the conductive case of test equipment. Both of these conditions are undesirable. Common mode currents flowing on the cable are of particular concern when testing electrically small antennas, as the feeder acts as an electrically long antenna element. This can reduce the resonance frequency of the antenna producing misleading test results.

In order to reduce the effect of common mode current, a ferrite sleeve was placed over the coaxial feeder close to each antenna's feed point.

[15] Precision terminations are required to create known "open", "short" and "50 Ω" terminated conditions at the end of the test cables so that the VNA can compensate for the distortion effects of the cables.

5. Evaluation of Multiband Antenna Designs Using High Impedance Feed-points

5.1 Introduction to Off-Centre Feed Dipoles

A half-wave centre-feed dipole in free space has an input impedance of 72 Ω at its fundamental resonance frequency. The impedance is resistive (i.e. real) with a low reactive (imaginary) component. The antenna presents similar input impedances on odd[16] harmonic frequencies, resulting in a good impedance match to 72 Ω. On even harmonic frequencies the antenna has high impedance, resulting in a poor match. This is demonstrated in Figure 6, which shows S_{11} for a centre-feed dipole as a red trace and S_{11} for an off-centre-feed (OCF) dipole as a blue trace.

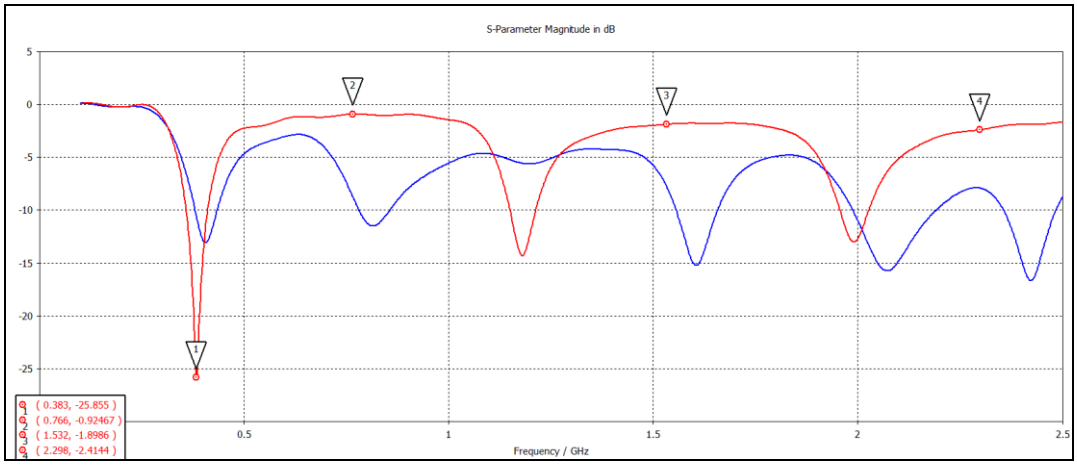

Figure 6: The S_{11} plot for a dipole antenna. Red trace: Centre-fed with 72 Ω impedance. Blue trace: Off-centre feed with 200 Ω impedance.

The fundamental resonance, labelled "1" in the graph, provides a reasonable match for both centre and Off-centre feed arrangements (S_{11} is better than 10 dB for both curves). The centre-feed dipole is a poor match on the even harmonics, labelled "2", "3" and "4", as S_{11} is worse than 2.5 dB in each case. The OCF dipole (blue trace) is a much better match on even harmonic frequencies.

As discussed in Section 4, the bands of interest for implantable antennas are 401 - 406 MHz and 2.4 - 2.5 GHz. An even[17] harmonic of the 401 - 406 MHz band falls within the 2.4 - 2.5 GHz band. Consequently a feed point located at the centre of a dipole would not provide an acceptable impedance match for both bands.

For the antenna to radiate efficiently it must present resistive impedance on both bands, with minimal reactance, and the resistances should ideally be similar in magnitude. This would allow the antenna to be easily matched to the implant's transmitter on both bands.

[16] In this context "odd harmonics" are considered to be odd multiples of the fundamental frequency.
[17] The 6th harmonic of the 401 - 406 MHz band is the band 2406 - 2436 MHz.

Early antenna designs that were developed for this thesis focused on a multi-band approach known as "Off-centre Feeding". This was the approach used to generate the blue trace in Figure 6. It can be seen that the blue trace has 5 resonant frequencies, while the red trace (centre feed) only has 3. The OCF approach is borrowed from amateur radio designs, which achieve acceptable antenna efficiency and impedance matching across a number of harmonically related bands.

At its fundamental resonance, the feed point impedance of a dipole is lowest at its centre and approaches infinity towards its open ends. Varying the feed point location allows the antenna to be used on its fundamental frequency and on its 2^{nd}, 4^{th}, 5^{th} and 6^{th} harmonics. Typically a distance 20% to 30% away from one end is often chosen, as at this location the dipole presents a resistive impedance of circa 200 Ω on all of these frequencies with low reactance.

The OCF design has some limitations. It is clear from Figure 6 that operation on the 3^{rd} harmonic is degraded and impedance matching a 200 Ω feed point impedance to a 50 Ω or 72 Ω transmission line requires a 4:1 transformer.

5.2 Modelling Off-Centre Feed Dipole Impedance Matching in CST

An Off-Centre Feed (OCF) dipole was modelled in free space using CST in order to demonstrate both its multi-band impedance matching and to investigate the effect of varying the signal source impedance. The dipole was 370 mm long with a feed point located 30% along its length. The source[18] impedance connected at its feed point was varied between 150 Ω, 200 Ω and 300 Ω in three successive simulations.

The effect of the three different source impedances on S_{11} is shown in Figure 8. There is a trade-off between S_{11} performance at the fundamental resonance (circa 400 MHz) and the 6^{th} harmonic at 2.4 GHz. Changing the impedance to improve one degrades the other. This indicates that the optimum feed point locations for these two frequencies are not precisely co-located. Notwithstanding, an acceptable S_{11} of circa 15 dB for both bands is achievable with an impedance between 150 Ω and 200 Ω.

All five resonances increase in frequency with rising source impedance, most notably the resonance just above 2 GHz.

[18] The CST discrete port which is shown as a red cone in Figure 7.

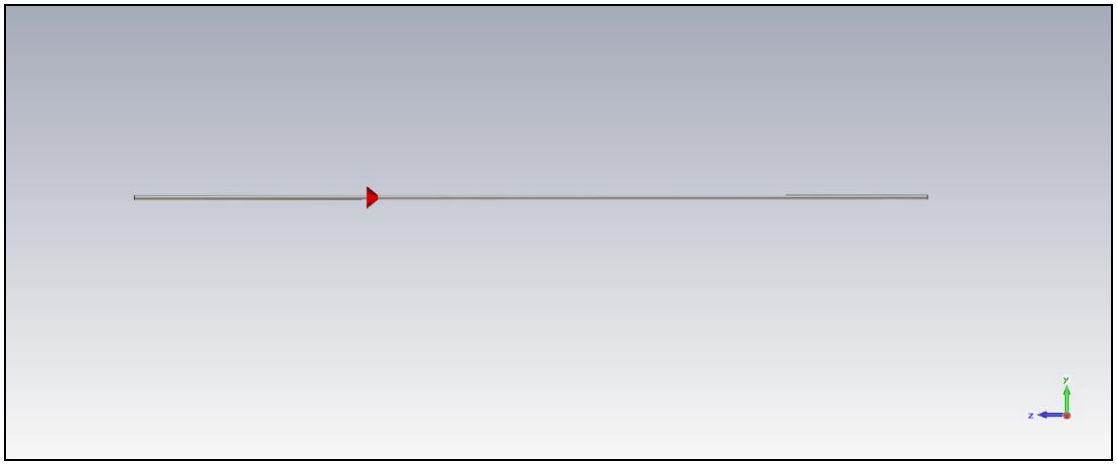

Figure 7: An OCF dipole antenna fed at a point located at 30% along its total length.

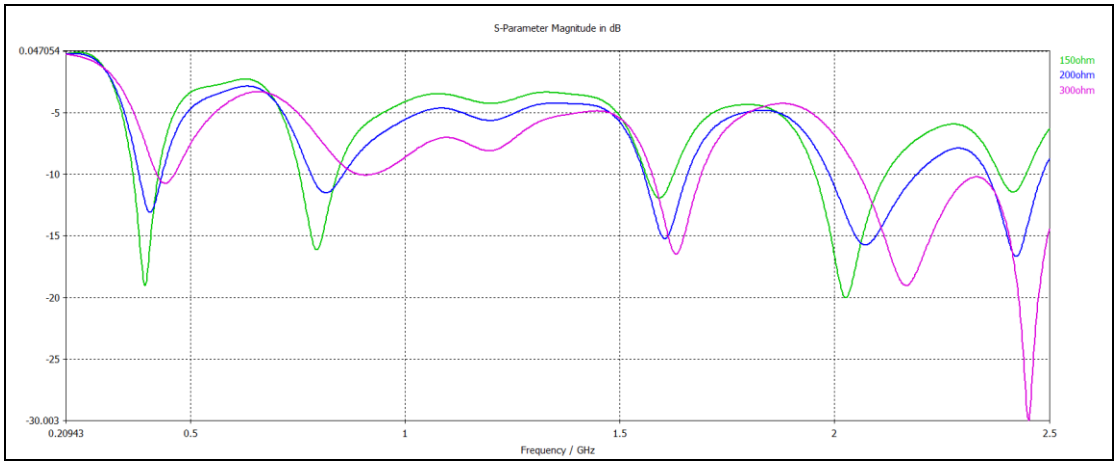

Figure 8: S_{11} of the antenna shown in Figure 7. The effects of three source impedances are shown: 150 Ω (green), 200 Ω (blue) and 300 Ω (purple).

Figure 9 shows the radiation pattern of the same antenna at its fundamental half-wave resonance frequency. It has a toroid pattern which is typical of a half-wave dipole in free space. It is evident that the feed point location has no significant impact on the dipole's radiation pattern, although in practice, the presence of a conductive feeder cable will perturb the pattern.

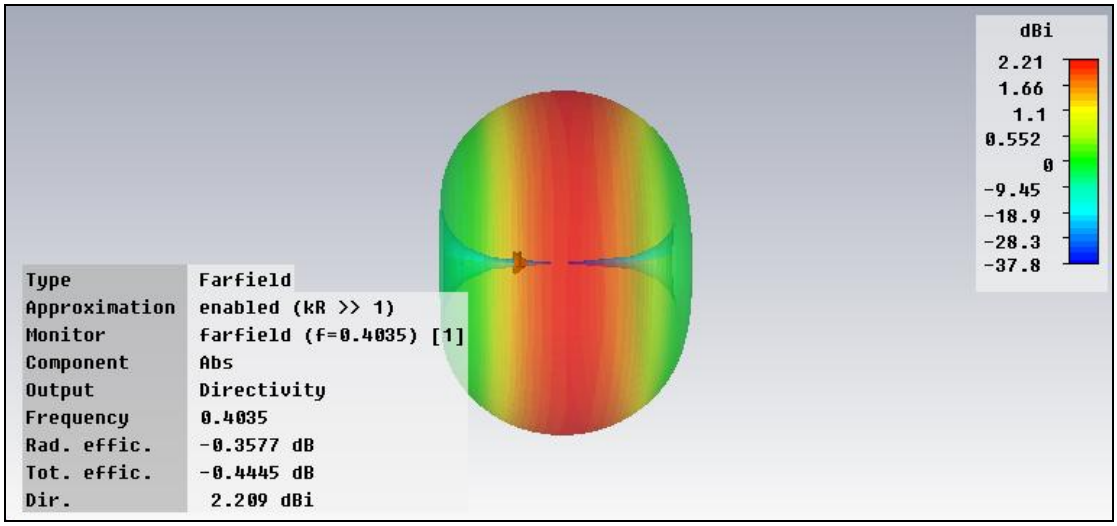

Figure 9: 403.5 MHz radiation pattern of the antenna in Figure 7.

At harmonic frequencies there are multiple standing waves along the length of the antenna causing it to radiate multiple lobes. Figure 10 shows the radiation pattern at 1.75 GHz with 3 distinct lobes.

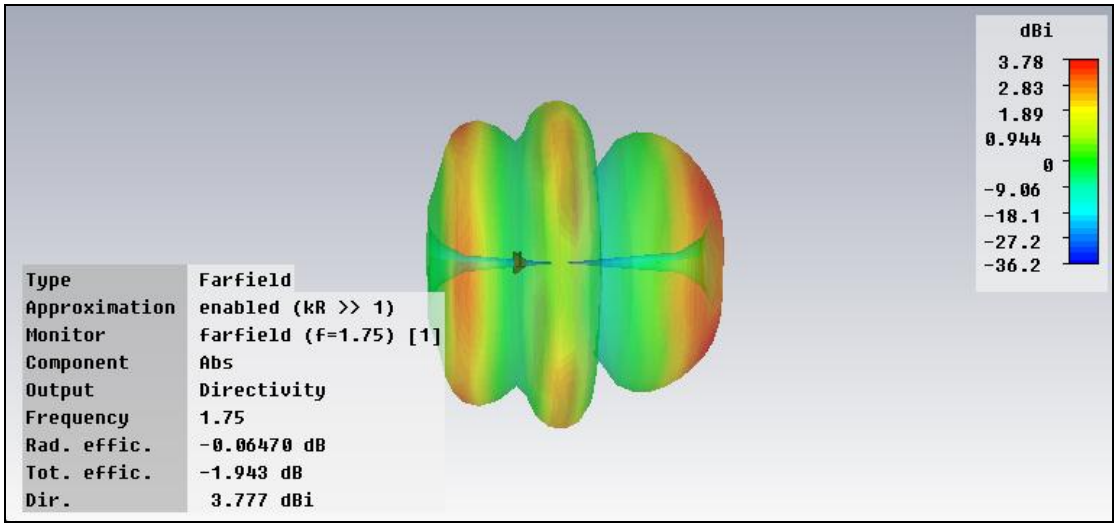

Figure 10: 1.75 GHz radiation pattern of the antenna in Figure 7.

5.3 Application of the Off-centre Feed Principle to Planar Inverted-F Antenna (PIFA) Designs.

This section presents the results of investigations into applying the off-centre feed multiband impedance matching approach to a PIFA design. Figure 11 below shows a CST model of a PIFA in free space. The ground plane measures 172 mm x 172 mm and the patch element measures 134 mm x 134 mm. They are separated by a 5 mm air space.

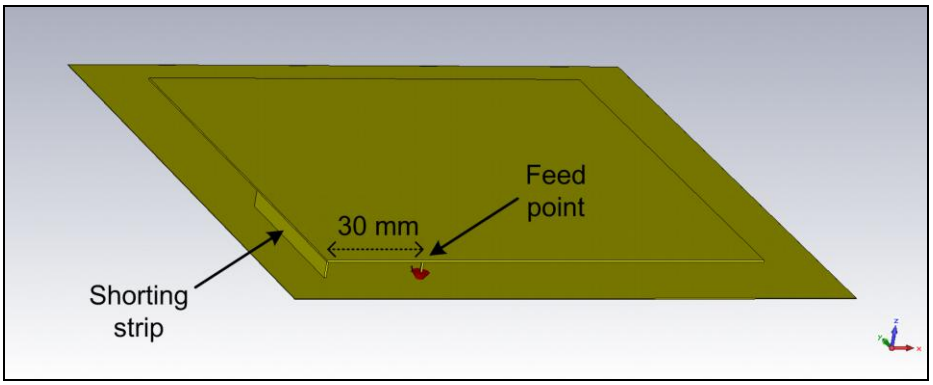

Figure 11: Physical construction of the PIFA.

The S_{11} simulation results show that the antenna model resonates in both the 401 - 406 MHz and 2.4 - 2.5 GHz bands. Two separate CST transient solver simulations were run with the source impedances of 50 Ω and 100 Ω. Figure 12 compares the results for the two impedance values. The antenna is a better match to a 100 Ω source, with an improvement of 13 dB at 403 MHz and 3 dB at 2.4 GHz compared to S_{11} for a 50 Ω source.

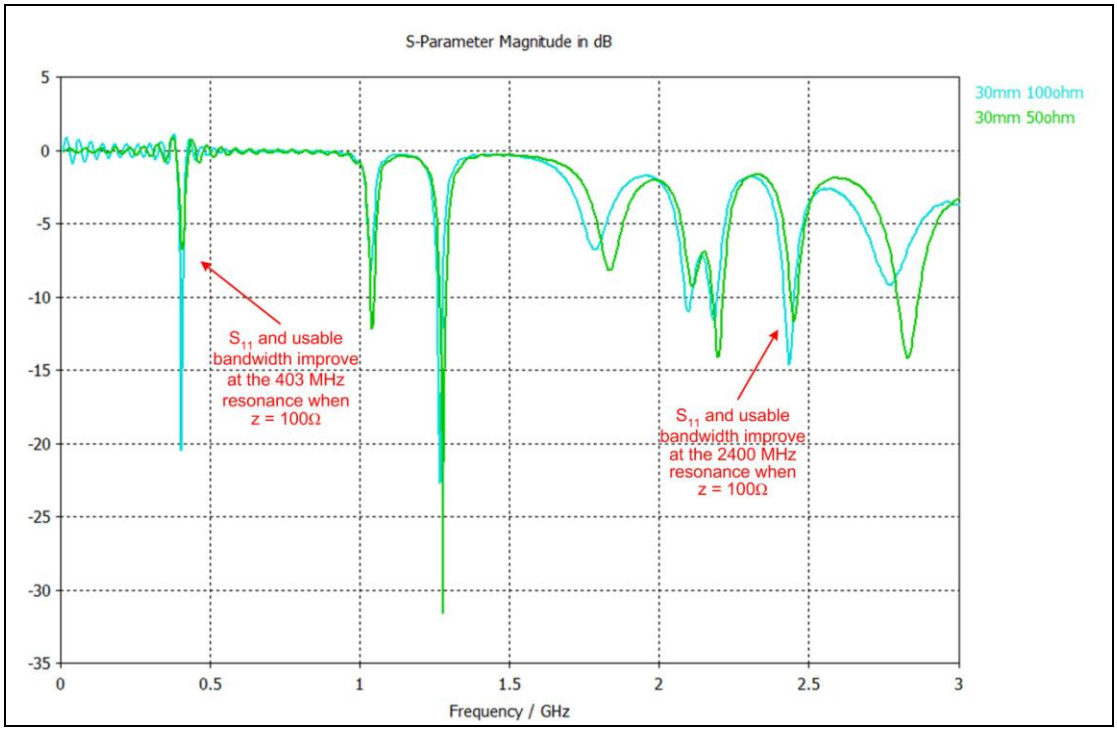

Figure 12: S_{11} results for the PIFA design shown in Figure 11 with source impedances of 50 Ω (green) and 100 Ω (blue).

5.4 The Effect on S_{11} When the Location of a PIFA Feed Point is Changed

The feed point of the PIFA in Figure 11 is located 30 mm from the shorting strip on the X-axis direction. The feed point impedance of a PIFA can be varied by moving the feed point closer to, or further away from, the shorting strip. Figures 13 and 14 present respectively the 403 MHz and 2.4 GHz results for S_{11} at various distances between the feed point and the shorting strip (between 20 mm and 30 mm).

It can be seen that the best match to a 100 Ω port is achieved at distances of 26 mm for 403 MHz and 30 mm for 2435 MHz. 28 mm is a reasonable compromise, providing S_{11} of 24 dB at 405 MHz and 12 dB at 2435 MHz.

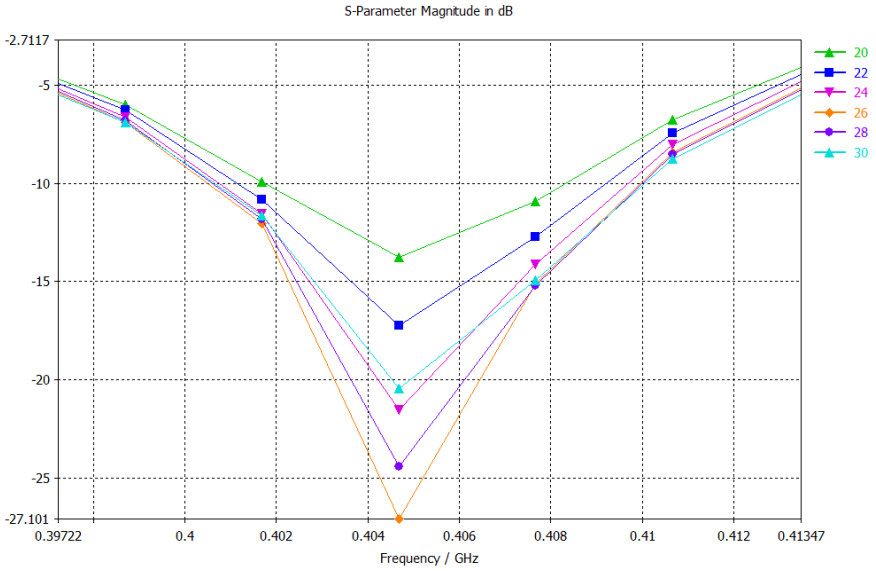

Figure 13: S_{11} at 403 MHz for various distances between the shorting strip and feed point. The source impedance is 100 Ω.

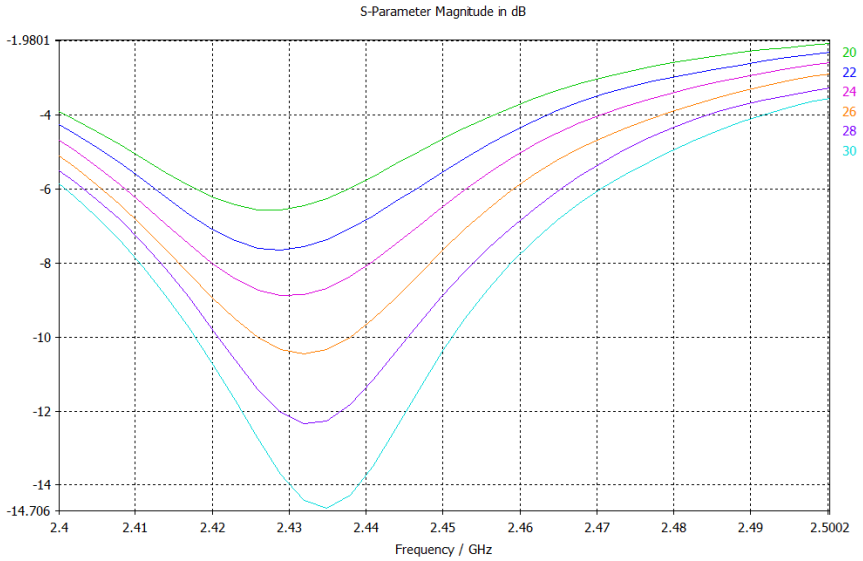

Figure 14: S_{11} at 2.4 GHz for various distances between the shorting strip and feed point. The source impedance is 100 Ω.

5.5 The Effect of Multi-band Operation on the Radiation Pattern of a PIFA

At its fundamental resonance frequency, the PIFA shown in Figure 11 has a single large lobe in its radiation pattern as presented in Figure 15. Figures 16 and 17 show that the radiation pattern develops three distinct lobes when the PIFA radiates at the 2.4 GHz harmonic. This behaviour[19] is similar to the OCF dipole radiating example shown in Figure 10.

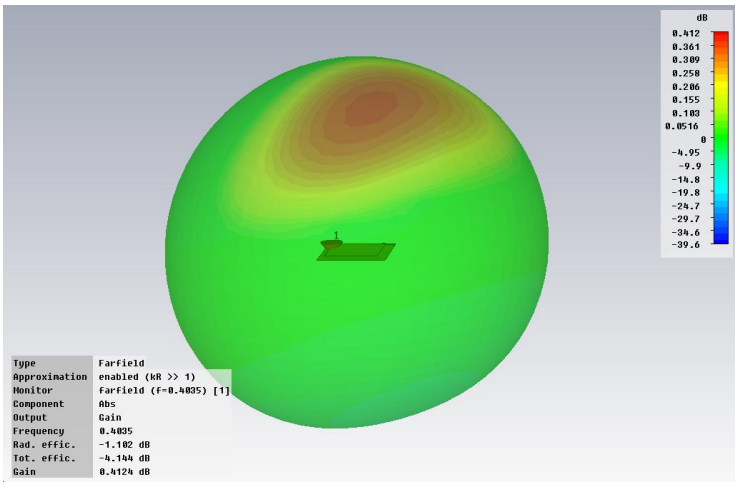

Figure 15: PIFA radiation pattern at 403.5 MHz.

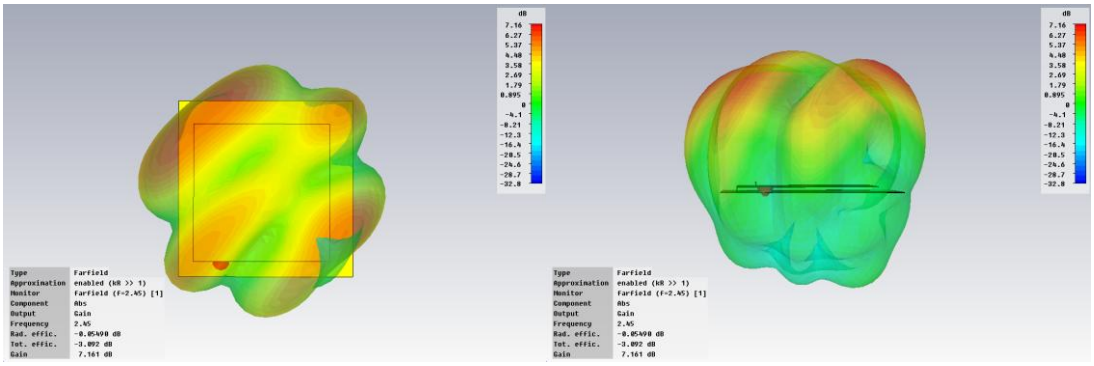

Figure 16: PIFA radiation pattern at 2.45 GHz viewed along the axis of the antenna (left) and close to the plane of the antenna (right).

[19] Note that the dipole is radiating its 4th harmonic in Figure 10 while the PIFA is radiating its 6th harmonic in Figure 16.

5.6 Conclusions on OCF Multi-band Antenna Designs

While the above results show promise for multi-band impedance matching, the OCF does have practical drawbacks for implant antennas, so high impedance multiband antenna designs were not further developed in this thesis. The two main factors influencing this decision were:

1. an impedance matching mechanism is required to adapt high antenna impedances, such as 200 Ω, to typical 50 Ω RF circuits. This can be done using discrete components (transformers) or using microstrip impedance matching. However the inclusion of additional matching components is undesirable. Space for components inside the implant is scarce and the inclusion of additional components means less space would be available for the antenna itself. Making the antenna electrically smaller to accommodate matching components would further reduce its efficiency and may negate the benefit of adding extra matching components.

2. The power budget is most critical in the 401 - 406 MHz band, where implants communicate with low power levels[20]. By contrast, the 2.4 GHz band is only used to "wake" the implant. The implant only needs to detect the presence of a 2.4 GHz signal, the source of which is located outside the body where ample electrical power is available. Moreover, much higher transmit power levels[21] are permitted in the 2.4 GHz band than in the 401 - 406 MHz band. The power budget is therefore far less critical for the 2.4 GHz band, where transmit power can be increased to mitigate inefficiency in the implants antenna performance and any additional loss incurred at the higher frequency.

With regard to these factors, it is preferable to prioritise the antenna's performance in the 401 - 406 MHz band where the power budget is most critical. Reduced performance in the 2.4 GHz band is acceptable as the power budget is less critical. It is also preferable to design an antenna with a 50 Ω feed point impedance.

[20] Transmitted power is limited to a maximum EIRP of 25 μW in the 401 - 406 MHz band, however practical considerations such as finite battery capacity may impose even stricter constraints on the implant's transmitted power level.

[21] Transmitted power is limited to a maximum EIRP of 10 mW for non-specific Short Range Devices in the 2400 - 2483 MHz band and 10mW for Healthcare Devices in the 2483 and 2500 MHz band.

6. Antenna Miniaturisation Techniques Applicable to Implant Designs

This section describes the effect of body tissue on antenna size and practical design techniques that can be used to further reduce the space requirements of an implantable antenna.

The wavelength of a 403 MHz electromagnetic wave in free space is calculated by:

$$\lambda_{\text{free space}} = \frac{C}{\text{frequency}} = \frac{3 \times 10^8}{403 \times 10^6} = 74.4 \text{ cm}$$

A half wave dipole for a wavelength of 74.4 cm would be close to 35 cm in length. Such a large antenna would be impractical for use inside the body. Therefore, practical implant antennas for the 401 – 406 MHz band must be small in comparison to the free space wavelength.

2 techniques were used to reduce the size of the antennas developed for this thesis. These were dielectric loading, adding reactance in the form of series inductance (meandering) and parallel capacitance (top hats).

6.1 Dielectric Loading

The wavelength of an electromagnetic wave travelling in a high dielectric medium is shorter than its equivalent in free space. The wavelength in the dielectric medium is determined by the following relationship:

$$\lambda_{\text{loaded}} = \frac{\lambda_{\text{free space}}}{\sqrt{\varepsilon}}$$

Where $\lambda_{\text{free space}}$ is the wavelength in free space, λ_{loaded} is wavelength in the dielectric medium and ε is the dielectric constant of that medium.

The value of ε inside the body typically varies between 30 and 50 depending on the tissue type encountered. This results in wavelength reduction factors of between 5.5 and 7.

Therefore the wavelength of a 403 MHz electromagnetic wave outside the body (74.4 cm) is shortened to between 13.5 cm and 10.6 cm inside the body. The size of an antenna's elements can be reduced proportionally when they are surrounded by body tissue.

6.2 Meanders, Series Inductance and Parallel Capacitive Loading

The space occupied by an antenna can be reduced by deforming its elements into meanders. Meandering adds series inductance and allows more efficient use of available space as it increases the length of the antenna elements that can be accommodated in a given area.

Alternatively series inductance can be added by using narrower conductors, with higher mutual inductance, as antenna elements.

These measures electrically lengthen the antenna, but they reduce radiation efficiency and usable bandwidth.

Parallel capacitance can be added close to the open end of a monopole to increase its effective length. This is done by adding elements with a lot of surface area are by widening antenna elements. Capacitive loading also results in loss, but it does not constrain antenna bandwidth to the same degree as series inductive loading.

7. Antenna Feed Arrangements - Evaluation of Microstrip and Coaxial Transmission Lines

Microstrip feeders, including Coplanar Waveguides (CPW), were investigated during the early stages of this thesis. Crude prototype antennas were produced and tested using CPW feeds (See Appendix 5).

The difficulty with microstrip feeders in a high dielectric environment is that larger separation distances are required between the tracks in order to maintain the desired characteristic impedance. Two different approaches were investigated to optimise microstrip feeder performance:

1. Keeping the phantom and shroud material away from the transmission line so that the tracks could be closely spaced. This was difficult with liquid and gel based shrouds and phantoms. Repeatability issues also made it difficult to obtain reliable test results.

2. Fully immerse the transmission lines in the dielectric material and widen the track spacing accordingly to achieve the desired characteristic impedance. This is undesirable as the transmission line then occupies a significantly wider area on the printed circuit board (PCB). Simulation models also showed that the transmission lines radiated, which would add uncertainty to antenna test results.

Coaxial transmission lines are not influenced by immersion in dielectric materials. The differential mode fields are contained within the cable and so material around the cable does not change its characteristics. Coaxial lines are also simpler to interface to test equipment. Common mode current on the outer shield can cause detuning of resonant antennas, but this can be mitigated with a common mode choke. See discussion on ferrite chokes in Section 4.4.

Early in the design phase a decision was made to use coaxial lines instead of microstrip lines because they are more practical for test purposes.

8. Prototype Antenna Development

8.1 CST Modelling of an Early Prototype Design

An initial monopole antenna was designed with a ground plane measuring 51 mm x 20 mm on a 0.4 mm thick FR4 substrate. The shield of a rigid 50 Ω coaxial feeder was bonded directly to the ground plane.

A strait monopole element extended to the end of the substrate, beyond the edge of the ground plane. The monopole element was fed by the centre conductor of the coax. The antenna model was surrounded on all sides with a 2 mm thick glycerine dielectric layer to act as a dielectric shroud. Only the feeder protruded through the glycerine shroud[22]. The model is shown in Figure 17.

The antenna's wideband S_{11} performance was simulated using the CST transient solver. The results are shown in Figure 18. A single resonance is visible at 1.3 GHz with S_{11} of 15 dB.

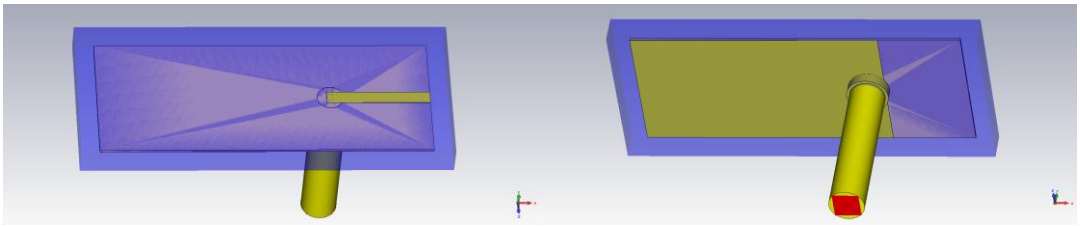

Figure 17: Diagrams of the antenna's upper monopole side (left) and its lower ground plane side with feeder (right).

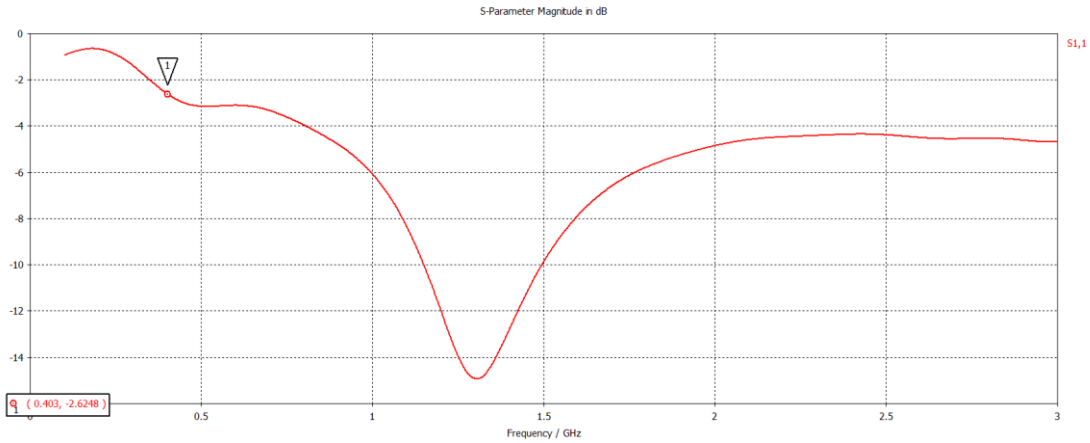

Figure 18: S_{11} of the monopole antenna shown in Figure 17 indicates resonance is at 1.3 GHz.

The initial antenna design was electrically short and the 1.3 GHz resonance frequency was more than 3 times that of the desired band (401 - 406 MHz). The Smith chart in CST (not shown) indicated that while the reactance was low at 403 MHz, the

[22] The red square that is visible at the end of the coaxial feeder is the waveguide port that excites the antenna model during the CST simulation. This port performs a similar role to the discrete ports (red cones) used to vary the source impedance in the simulations described earlier.

radiation resistance of 7.5 Ω was much too low to efficiently match it to a 50 Ω device. S_{11} at 403 MHz was only 2.6 dB.

The antenna was electrically lengthened by adding meanders and "capacitive hat" loading to its monopole element. This was done over 13 different stages, each comprising a design change and a CST simulation to analyse its effectiveness. The main changes are summarised below.

In Figure 19 the monopole element was shaped into an inverted-L with a parallel meander section. This increased the element's physical length from 15.5 mm to 40 mm and reduced its resonant frequency from 1.3 GHz to 676 MHz. The monopole's protrusion distance beyond the edge of the ground plane was also shortened by 4 mm, reducing the PCB area required. S_{11} at 403 MHz was improved by 1.5 dB, but it remained poor at only 4 dB.

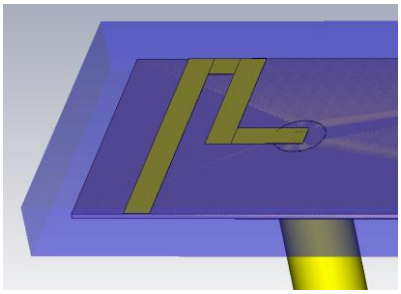

Figure 19: The meandering Inverted-L monopole.

In Figure 20 a further meander section was added to the monopole element, providing an additional 8.5 mm of length. A "capacitive hat" area of 28 mm^2 was added directly above the ground plane. The capacitive hat and ground plane form two plates of a capacitor, separated by 0.4 mm of FR4 substrate with an ε value of 4.3.

The hat provides an additional 2.7 pF of parallel capacitance. Locating the hat section directly over the ground plane increases the capacitance achieved for a given area of PCB space. It is an efficient way of adding capacitance, while preserving PCB space for other implant systems. It also increases undesirable loss in the antenna, as at 403 MHz it appears as a -146 Ω path to ground. However its inclusion cancels unwanted reactance and improves the antenna's S_{11} at 403 MHz to 12 dB, so RF power is more efficiently delivered to the antenna. Overall, the 8 dB improvement in S_{11} mitigates the loss associated with the capacitive hat.

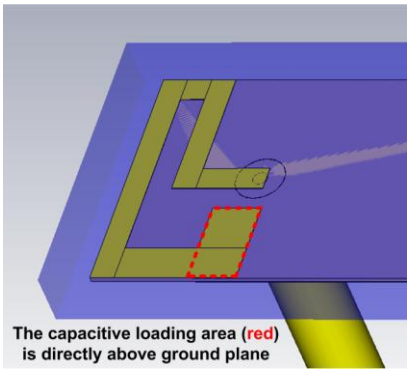

Figure 20: Further meandering and the capacitive hat (highlighted in red).

The V47 model

In figure 21 a final meander section was added, bringing the resonant frequency to 403 MHz. The full 401 to 406 MHz band has S_{11} of better than 14 dB. RF current in the final meander section flows in the opposite direction to the section immediately before the capacitive hat. This is not good practice in general, as nearby currents flowing in opposite directions reduce desirable mutual inductance in the antenna elements and also cause some far field cancellation. However, in this case the parallel sections are close to the high impedance (open) end of the monopole, where current flow is reduced. The capacitive hat also ensures that current flow in the final section is further reduced, mitigating the effect of the opposing currents.

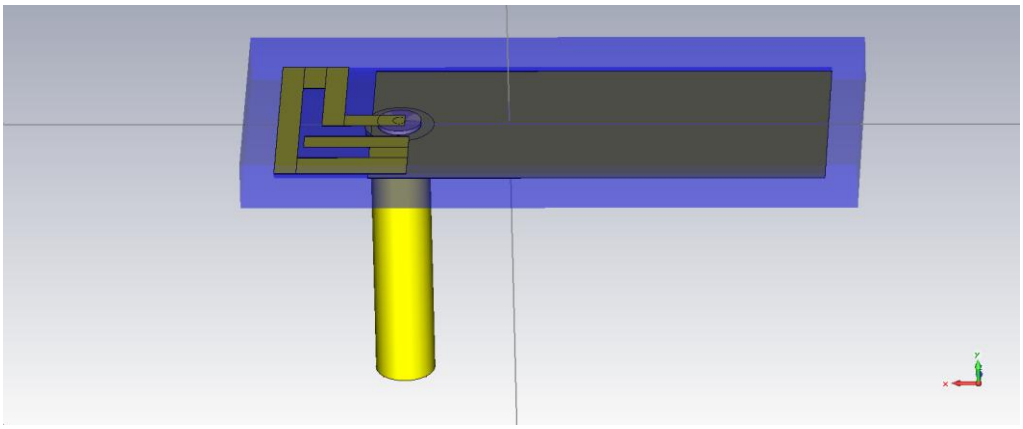

Figure 21: The V47 model used to produce a handmade prototype.

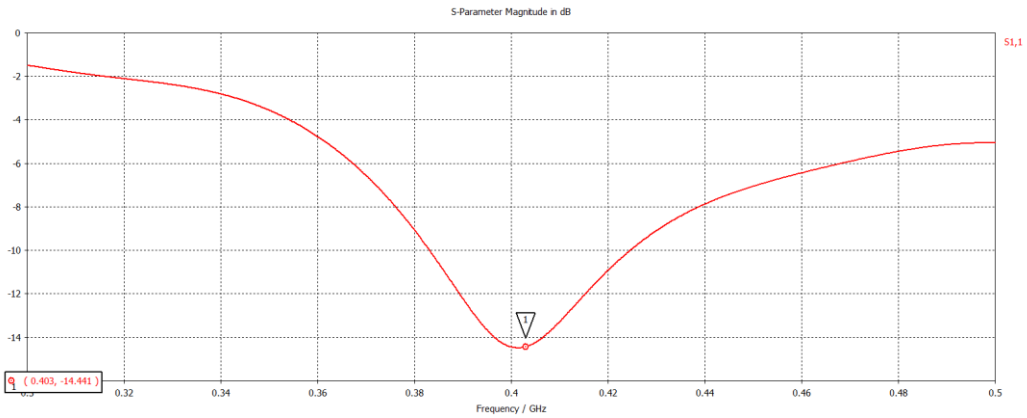

Figure 22: The V47 model with S_{11} of 14 dB, centred on 403 MHz.

8.2 Early Handmade Prototype

A crude initial prototype antenna was produced on FR4 substrate with a single-sided copper layer. The copper layer formed the ground plane while the active element was cut by hand using adhesive copper tape. A 250 mm long section of 2.2 mm diameter rigid coaxial cable was used to feed the prototype. It is shown in Figure 23 below.

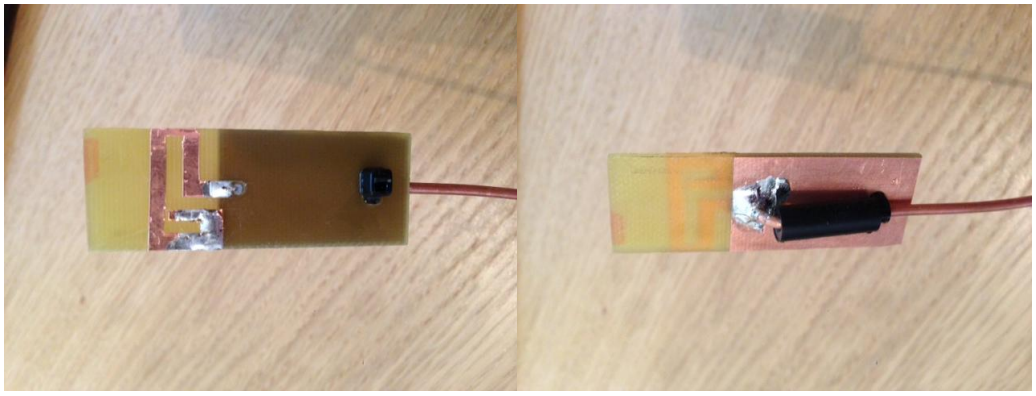

Figure 23: The initial handmade prototype, showing the monopole side (left) and the ground plane side and coaxial pigtail (right). The black object on the pigtail is a ferrite common mode choke.

The prototype was immersed in a glycerine shroud and placed inside a pork phantom lined with 12 µm thick PVC film. The VNA measurement results for the initial prototype did not agree with the CST predictions for S_{11} performance. The S_{11} plot in Figure 24 below indicates that there was no resonance point anywhere between 350 MHz and 650 MHz when glycerine was used.

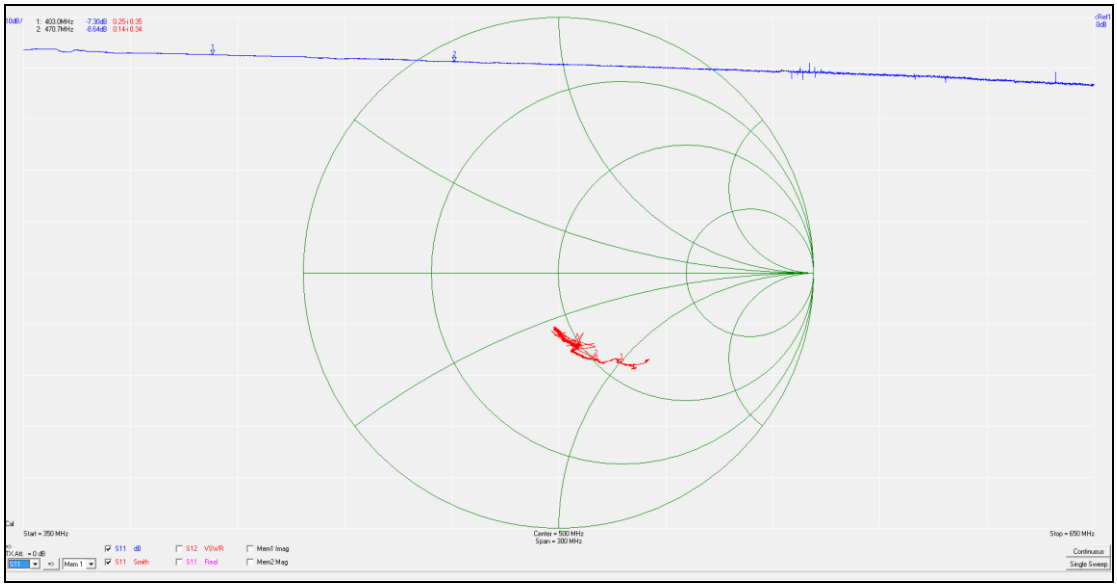

Figure 24: Plot of S_{11} for the initial prototype (Figure 6) in a pork phantom **with** a glycerine shroud. No resonance is visible between 350 MHz and 650 MHz.

The prototype was retested without the glycerine using only PVC film as an insulating shroud. Under these conditions the antenna resonated at 620 MHz with S_{11} of 45 dB, but S_{11} at 403 MHz was only 7 dB. The S_{11} results are shown in Figure 25.

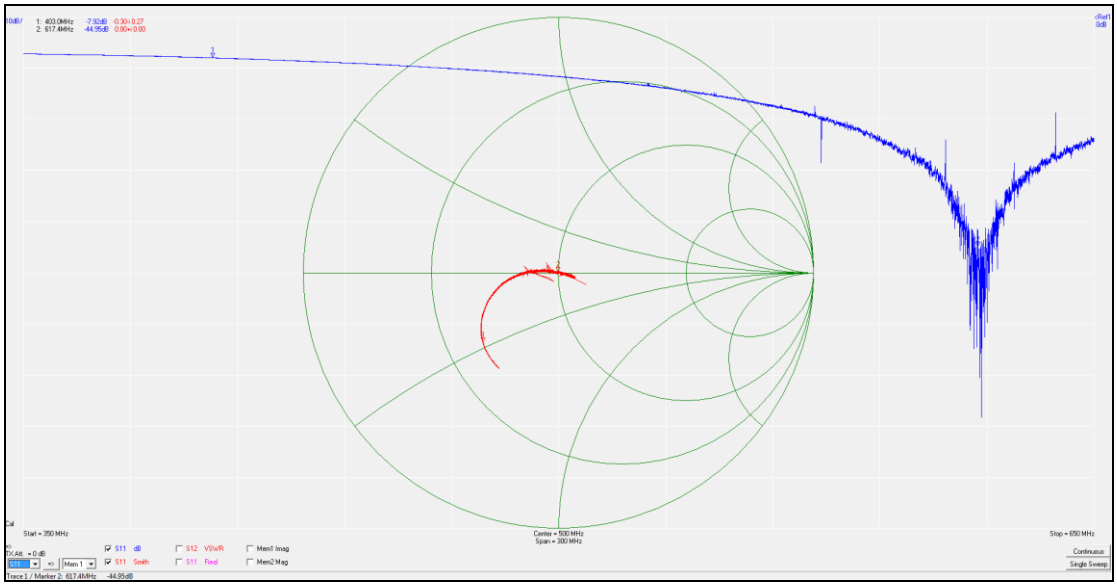

Figure 25: Plot of S_{11} for the initial prototype (Figure 6) in a pork phantom **without** a glycerine shroud. (PVC film insulation only).

The prototype was later empirically modified by cutting additional notches into the monopole element. It was again tested and its resonant frequency had been reduced by 70 MHz. Figure 26 shows the resonance at 550 MHz with S_{11} of 34 dB.

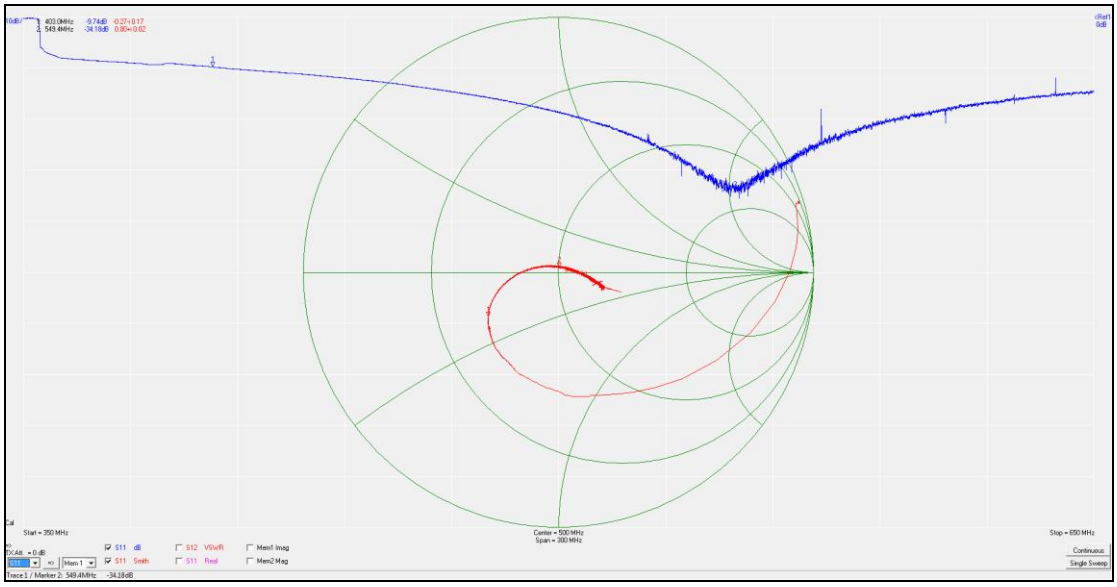

Figure 26: Plot of S_{11} for the empirically modified prototype in a pork phantom **without** a glycerine shroud. (PVC film insulation only).

8.3 The First Milled Prototypes

Two further variants of the V47 model were designed and simulated in CST and prototypes were printed under controlled conditions using a CNC milling machine.

The V49 Model: This was almost identical to the V47 model used to produce the initial handmade prototype. The Smith chart on the right is S_{11} predicted by CST.

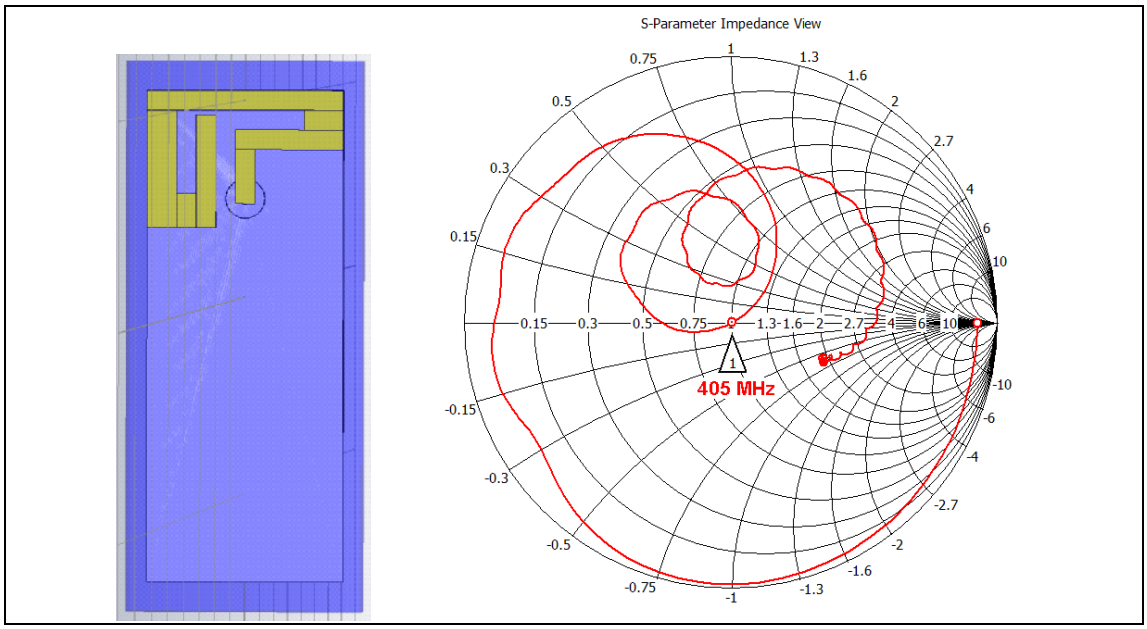

Figure 27: The V49 CST model.

The V50 Model: The final meander section was modified in this model and it included a capacitive hat area of 33 mm^2 to improve S_{11} at 403 MHz. The Smith chart on the right is S_{11} predicted by CST.

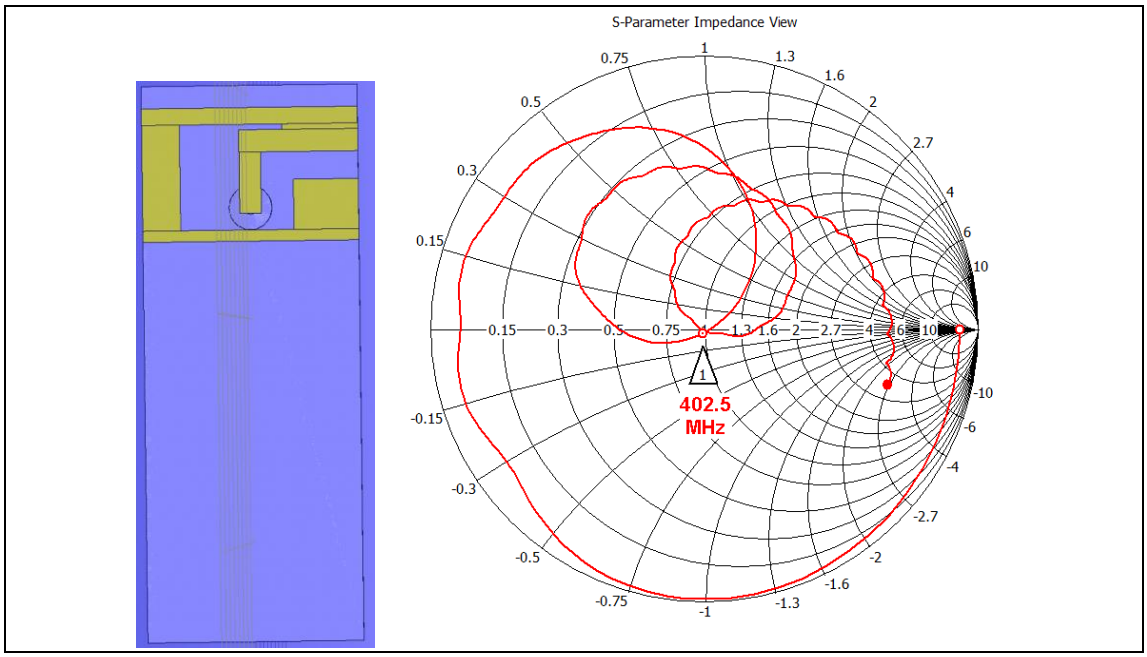

Figure 28: The V50 CST model.

The V49 and V50 prototypes were tested with a Rohde & Schwarz VNA, both with and without glycerine shrouds. The performance was again poor using the glycerine shrouds. However, when the glycerine shroud was removed, the frequency response of the prototypes agreed closely with the CST predictions. Figures 29 and 30 compare the VNA results (blue) with the CST simulation results (red). It is evident from these plots that for both prototypes there was an offset in the resonance frequency. For V49 and V50 the offsets were 139 MHz and 157.5 MHz respectively.

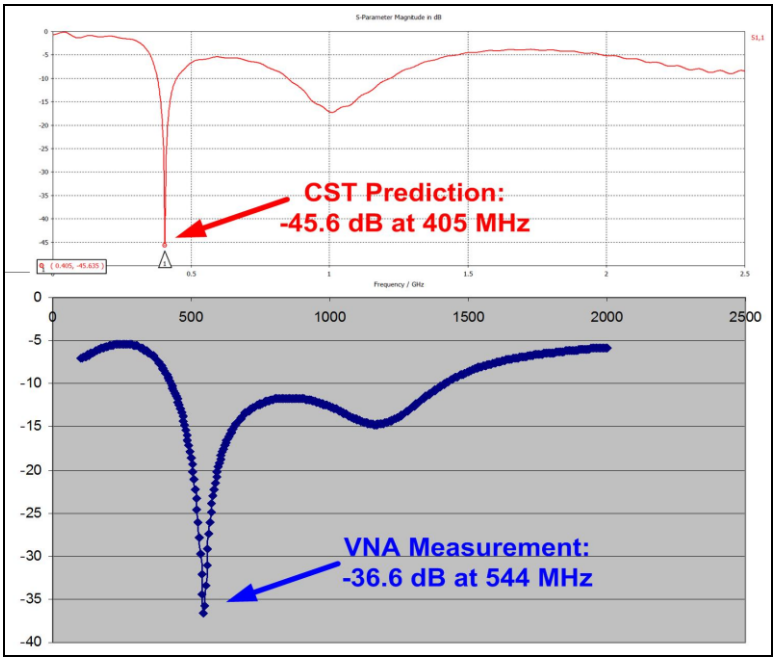

Figure 29: Plot of S_{11} for the V49 prototype in a pork phantom **without** a glycerine shroud. (PVC film insulation only).

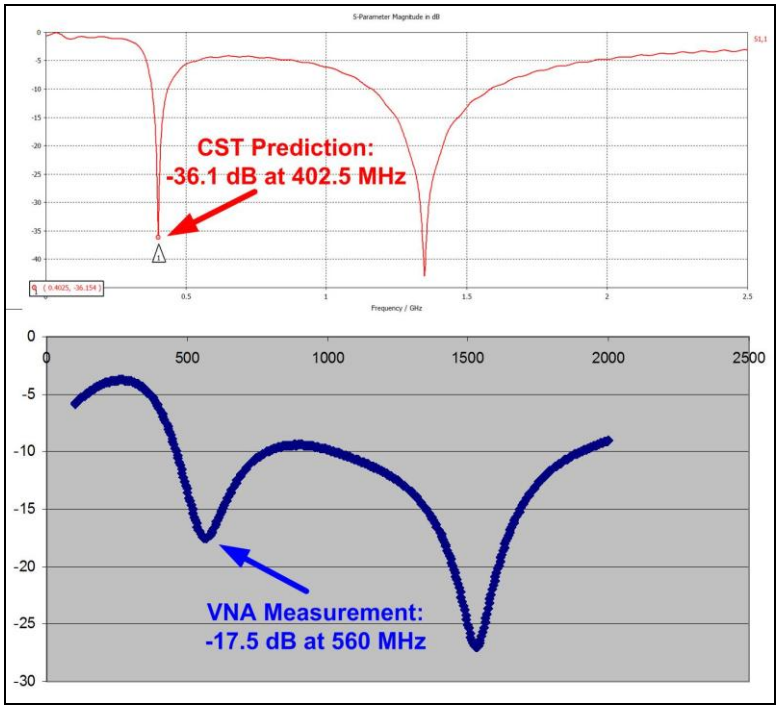

*Figure 30: Plot of S_{11} for the V50 prototype in a pork phantom **without** a glycerine shroud. (PVC film insulation only).*

8.4 Analysis of Unexpected Measurement Results

Figures 29 and 30 in the previous section highlight the difference between the resonant frequencies predicted by the transient solver in CST and that of the prototypes when measured with the VNA. This frequency discrepancy affected both of the milled antenna designs. The previous handmade prototypes, albeit produced under less controlled conditions, also resonated at higher frequencies than predicted. This deviation from the predictions warranted further analysis.

There were a number of possible sources of error that were suspected of contributing to the frequency offset. These were:

- Variations between the dielectric properties of the phantom tissue used in the simulations and that used in the VNA testing.
- The effect of common mode current flowing on the outside of the coaxial feeder.
- Errors in the configuration of the CST simulation.

Appendix 3 presents the full results of further CST simulations that were run to determine if the 3 above factors were causing the frequency deviation.

The conclusions drawn from these investigations were as follows:

Investigation 1 - The impact of variations in the phantom material and its effect on antenna resonant frequency.

The V49 antenna model was simulated with 5 different phantom material types. Plain tap water and 4 different body tissue types (skin, brain, bone and fat) were selected to provide a diverse range of electrical characteristics in the simulations. The resulting S_{11} frequency response plots are presented in Appendix 3, and summarised below in Table 1 along with the phantom material characteristics used in each simulation. The impact on the antenna's resonant frequency is also listed.

Phantom material	Dielectric constant (Epsilon)	Magnetic permeability (Mue)	Electrical conductivity	Antenna resonance frequency	**Deviation from 405 MHz**
Skin	31.29	1	8.0138 S/m	405 MHz	**0 MHz**
Brain	38.111	1	10.31 S/m	405 MHz	**0 MHz**
Bone	12.66	1	3.8591 S/m	418 MHz	**+ 13 MHz**
Tap Water	78	0.999991	1.59 S/m	437 MHz	**+ 32 MHz**
Fat	4.6	1	0.58521 S/m	524 MHz	**+ 119 MHz**

Table 1: The effect of various phantom materials on antenna resonant frequency.

Despite the diverse characteristics of the phantom materials used, none of the simulations resulted in frequency deviations similar to that observed during the VNA measurements[23]. Fat tissue, which caused the greatest deviation, is a statistical outlier.

[23] For V49 and V50 the frequency discrepancies were 139 MHz and 157.5 MHz respectively.

Its low water content gives it a very low dielectric constant with respect to other body tissues. Even tap water produced a deviation of only 20% to 25% the size of the measured offset in the VNA tests.

After considering these results, phantom material variation was dismissed as a cause of the measured frequency offset.

Investigation 2 - The effects of common mode current on the coaxial feeder.

Two different versions of the V49 model were simulated in CST with differing lengths of coaxial feeder (4 mm and 125 mm). The results are also presented in Appendix 3. While the extra coax did introduce additional loss, with a consequent increase of wideband return loss, it did not change the resonance frequency. It was also noted during the VNA measurements, that moving the ferrite choke along the length of the feeder had no noticeable impact on the antenna's resonant frequency. For these reasons the coaxial feeder was eliminated as a possible cause of the frequency offset.

Investigation 3 - Agreement between free space S_{11} predictions and measurements.

The S_{11} performance of the V49 model in free space was simulated and measured. Close agreement between the free space prediction data and measurements indicated that the CST tool is correctly configured. At higher frequencies there was a 2 dB return loss difference between the prediction and measurement data, however this can be explained by the higher insertion loss of the 15 cm thin coax feeder on the prototype. The CST model has a shorter feeder with a lower insertion loss. As a result of this exercise, errors in the construction of the CST antenna models were eliminated as a possible cause of the discrepancy.

Investigation 4 - Review of suitability of glycerine as a dielectric loading material.

The literature suggests that a layer of glycerine surrounding the antenna aids dielectric loading of the antenna and impedance matching to the surrounding high dielectric tissue [1]. The results of prototype tests so far indicated that this was not the case.

In order to determine if a glycerine shroud was necessary, two simulations were run, with and without a glycerine shroud. Both simulations use the same antenna and the same phantom. It was noted that there is only a 2 dB difference in radiation to the far field, and the model with the glycerine shroud had the greater loss. The results of the simulations are presented in Appendix 3.

8.5 Changes to the Research Methodology Arising from These Investigations

Using simulation software

The results of the investigation did not identify the cause of the frequency offset observed between the CST simulations and the VNA measurements. It was felt that it would be imprudent to continue adding further design refinements to simulation models which have unexplained variations in their results.

It was instead decided to further develop the prototypes empirically without the use of simulation software. Once antenna prototypes had been tested and validated, the designs could then be simulated again in CST. This would allow the simulation predictions to be reconciled with measurement results and to identify the cause of the frequency offset.

Review of glycerine as a shroud material

The early prototypes used glycerine which is marketed as a food additive, and its manufacturer claims that it contained no other substances. Nevertheless, although glycerine was suggested [1] as a low loss, high dielectric material suitable for shrouding, it had performed poorly in the measurement results so far.

PVC film provided promising results in some of the tests, but it inevitably traps small air pockets which lowered the dielectric constant in the antenna's near field. This caused the antenna's performance to vary depending on the pressure applied to it. Liquid or gel based shroud materials do have an advantage over PVC film in this regard, as the antenna can be fully immersed in the liquid without trapping any air.

The problem of trapped air was resolved by coating the prototypes in a thin layer of epoxy resin instead of PVC film and allowing it time to cure. Cured epoxy resin has a dielectric constant of 3.6 which is similar to that of PVC (3.4). This fully sealed the prototypes and prevented phantom material ingress.

It was decided not to use glycerine as an insulating shroud material in subsequent prototype designs and instead to encapsulate them in epoxy resin.

Review of artificial phantoms

Earlier prototypes were tested in phantoms made using fresh meat products (pork and chicken), or in some cases, hands clasped around an insulated antenna for proof of concept. However it proved difficult to maintain a controlled test environment using these methods.

When hands are used as a phantom small air gaps are trapped close to the antenna. Tests showed the antenna's frequency response and S_{11} to be highly sensitive to the pressure applied. Repeatability was very poor with this approach.

It is also difficult to control for such variation using meat products as a phantom. It is difficult to fully surround the antenna with meat so its performance is also sensitive to the pressure applied. Moreover, the characteristics of meat changes over time. These changes influence the prototype's performance and impair the repeatability of the test results. The meat did not have to spoil or dry out for there to be a noticeable effect on how it dielectrically loaded an antenna. Often there is no way to know how long a meat product has been on sale, and there were differences between some of the samples purchased for the tests.

It was decided to avoid using meat products and to use an artificial liquid based phantom in order to improve the repeatability of the test results. A phantom composed of de-ionised water, sugar, salt and HEC was selected. The recipe was taken from "Simulated biological materials for electromagnetic radiation absorption" by G Hartsgrove, A Kraszewski, A Surowiec - Bioelectromagnetics, 1987. The characteristics are described as dielectric constant of 49, mue of 1 and electrical conductivity of 0.6 S/m.

8.6 Empirical Retuning of Prototype Antennas.

The two milled prototypes were empirically retuned in order to bring their resonances from 544 MHz (V49 model) and 560 MHz (V50 model) down to the desired band of 401 – 406 MHz.

Two modifications were made to the V49 model:

- a 50 mm right-angled groove was scored close to the edge of the ground plane.
- a 40 mm section of 0.5 mm diameter copper wire was added by drilling a through-hole via at the end of the microstrip monopole, and routing it around the edge of the substrate.

The copper wire was trimmed by removing 1 mm at a time and retesting. Using this method the resonance was brought to 403 MHz with S_{11} of 22 dB.

Figure 31: The empirical modifications made to the V49 prototype monopole side (left) and ground plane side (right).

Two similar modifications were made to the V50 prototype:

- a 50 mm right-angled groove was scored close to the edge of the ground plane.
- a 30 mm section of 0.5 mm diameter copper wire was added around the edge of the substrate.

Again, the copper wire was trimmed incrementally and retested. The resonance was brought to 403 MHz with S_{11} of 38dB.

Figure 32: The empirical modifications made to the monopole side (left) and ground plane side (right) of the V50 prototype.

The CST antenna models were updated to incorporate the empirical modifications described above and new prototypes were milled. They were encapsulated in epoxy resin shrouds with thicknesses varying between 0.1 and 0.2 mm. The prototypes were assigned labels to identify them during the final validation measurements which are discussed in the next section.

- **Prototype A** - Milled using the modified **V50** model with a **17 mm** final meander section.
- **Prototype B** - Milled using the modified **V50** model with a **15 mm** final meander section.
- **Prototype C** - Milled using the modified **V50** model with a **13 mm** final meander section.
- **Prototype E** - Milled using the modified **V49** model.

The 4 final prototypes[24] are shown in Figure 33.

[24] A fifth "Prototype D" antenna was produced. It was milled using the modified V50 design with a 11 mm long final meander section. It was damaged prior to encapsulation in epoxy resin so the results have been excluded.

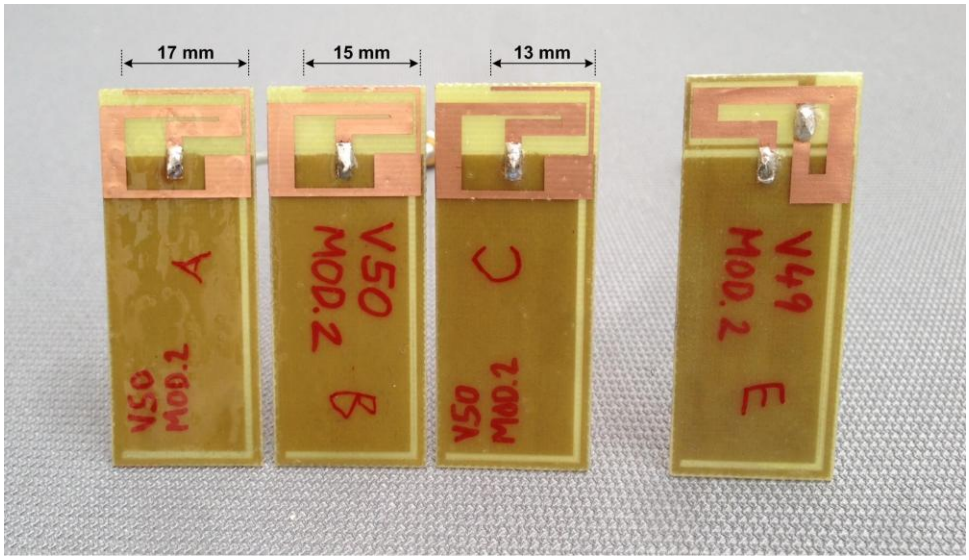

Figure 33: The final antenna prototypes. Prototypes A, B and C are variants of the V50 CST model, with different meander lengths as shown. Prototype E is a variant of the V49 CST model.

9. Validation Testing

The 4 antenna prototypes were immersed in the liquid phantom and tested with a 24 GHz Rohde & Schwarz ZVA Vector Network Analyser. The results are discussed in this section with reference to graphs of S_{11} performance. The full tabular S_{11} results are presented in Table 8 in Appendix 4 for reference.

9.1 Test Results for Prototypes A, B and C.

The S_{11} results for prototypes A, B and C are plotted in Figures 34 and 35 below.

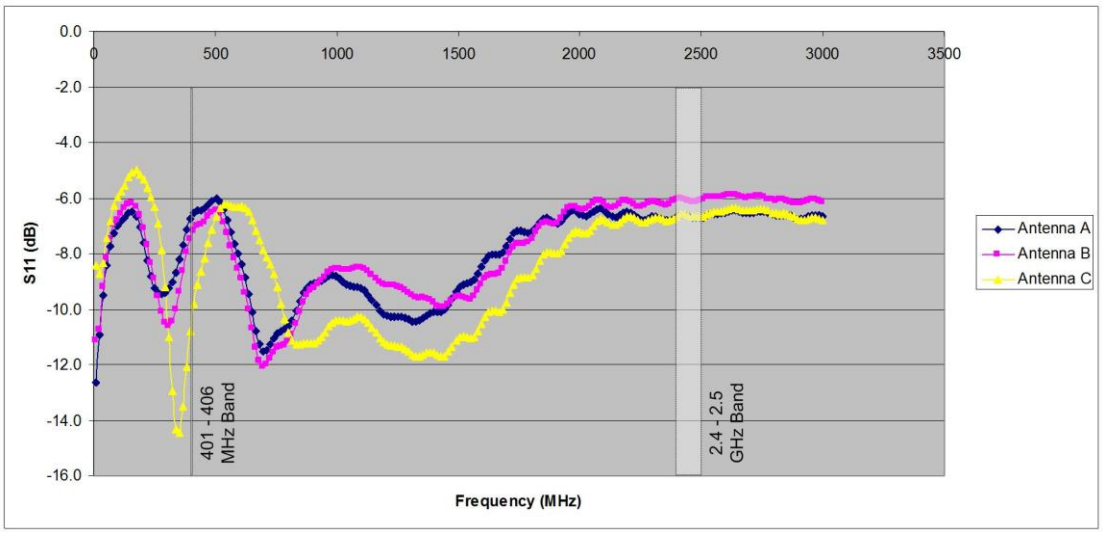

Figure 34: A graph of S_{11} performance for prototypes A, B and C between 10 MHz and 3 GHz. The desired bands of 401 - 406 MHz and 2.4 - 2.5 GHz are highlighted in light grey.

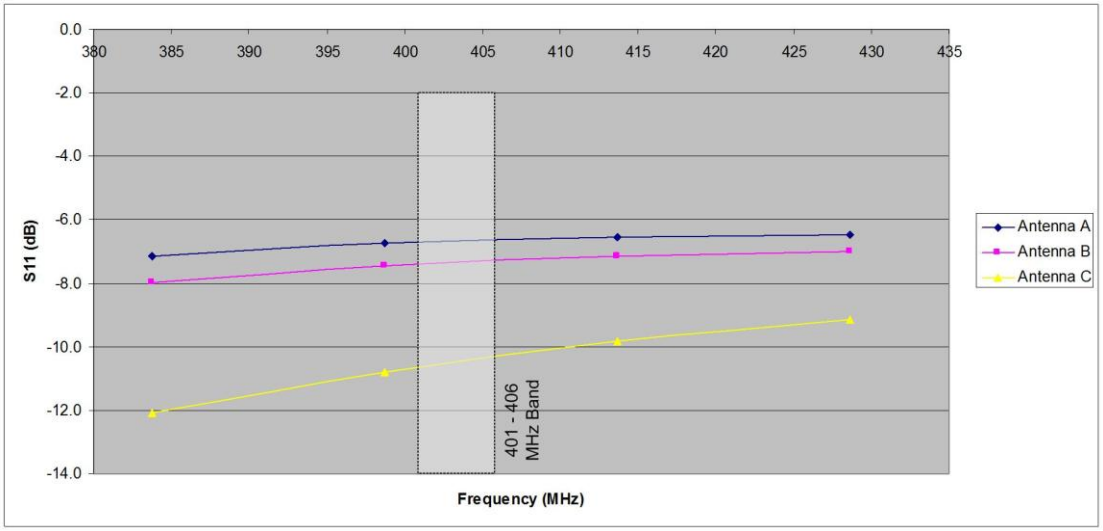

Figure 35: A graph of S_{11} performance for prototypes A, B and C between 380 MHz and 430 MHz. The desired band of 401 - 406 MHz is highlighted in light grey.

It is evident from Figures 34 and 35 that prototypes A, B and C are electrically too long for the dielectric loading conditions in the phantom, as all three resonate at frequencies below the 401 - 406 MHz band. It is notable that removing just 2 mm of track from the final meander increased the antenna's resonance frequency by between 30 to 45 MHz.

Prototype C, which had the shortest meander length (13 mm), has the closest resonance, but the 14.5 dB peak in S_{11} is 50 MHz below the desired band. It can be interpolated from the three resonance frequencies, that a meander length of 11 mm would bring the frequency of resonance close to the desired band.

The S_{11} performance of Prototype C in the 401 - 406 MHz band is acceptable at 10.3 dB. Prototypes A and B have inferior performance, but noting the short feeder lengths used in implants, their S_{11} performance of circa 7 dB may still result in acceptable feeder losses.

The results for the Prototypes A, B and C are summarised in Table 2.

Prototype	**Best S_{11} near the 401 - 406 MHz band**	**Worst S_{11} inside the 401 - 406 MHz band.**
A	9.5 dB at 279 MHz	6.6 dB
B	10.6 dB at 309 MHz	7.3 dB
C	14.5 dB at 354 MHz	10.3 dB

Table 2: Resonance frequencies and S_{11} performance of Prototypes A, B and C.

9.2 Test Results for Prototype E

The S_{11} results for prototype E are plotted in Figures 36 and 37 below.

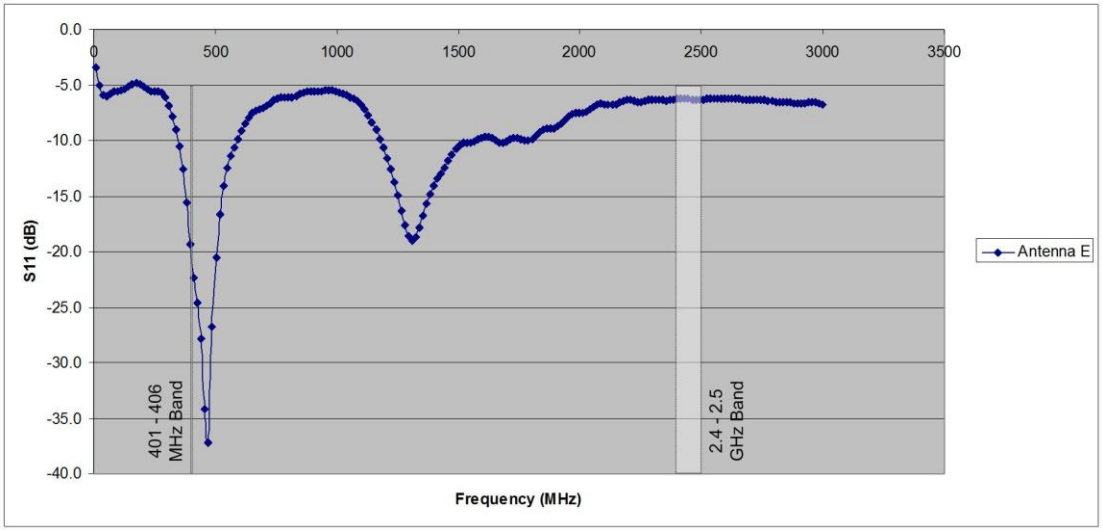

Figure 36: A graph of S_{11} performance for prototype E between 10 MHz and 3 GHz. The desired bands of 401 - 406 MHz and 2.4 - 2.5 GHz are highlighted in light grey.

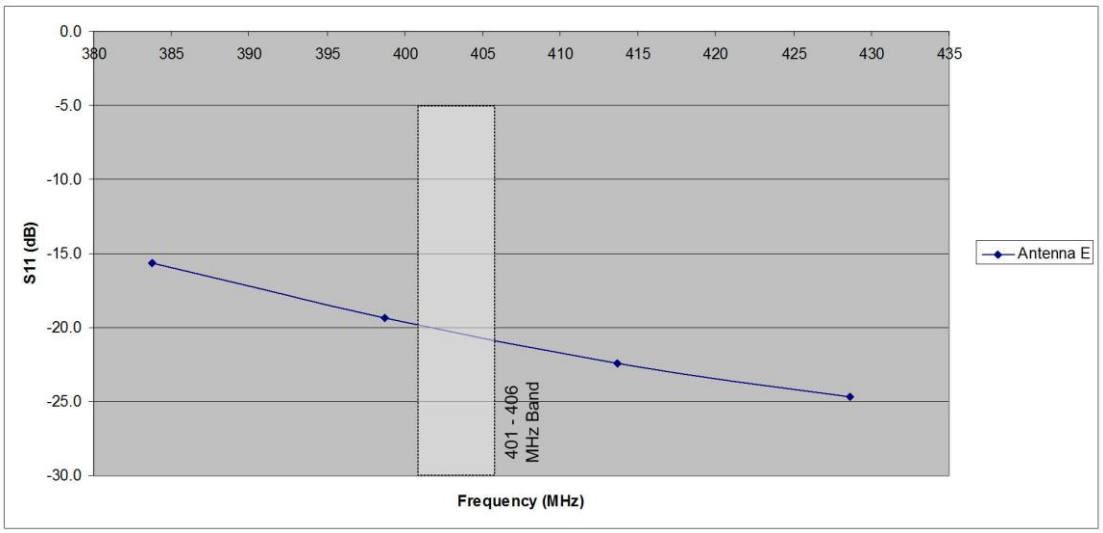

Figure 37: A graph of S_{11} performance for prototype E between 380 MHz and 430 MHz. The desired band of 401 - 406 MHz is highlighted in light grey.

Figures 36 and 37 indicate that prototype E is electrically short as its resonance is 70 MHz above the 401 - 406 MHz band. S_{11} performance within the 401 - 406 MHz band is favourable at 20 dB. S_{11} could be further improved, but it is unnecessary. Moreover it is difficult to add more electrical length to Prototype C's design in order to reduce its resonance frequency. Alternatively this could be achieved by adding series inductance (narrower elements) or parallel capacitance (top hats) to the design. However, doing so may also reduce the antennas usable bandwidth, making it more "location sensitive" when it is surrounded by tissues with different dielectric constants.

The results for Prototype E are summarised in Table 3.

Prototype	Best S_{11} close to the 401 - 406 MHz band	S_{11} within the 401 - 406 MHz band.
E	37.2 dB at 473 MHz	20 dB

Table 3: Resonance frequency and S_{11} performance of Prototype E.

9.3 Conclusions on the Validation Test Results

The antenna designs provided good results overall, achieving S_{11} of 10 dB to 20 dB in the 401 – 406 MHz band.

The resonant frequencies of the 4 prototypes varied widely[25]. This was not related to the simulation software issue described in Section 8.

The prototypes were based on a preceding generation of empirical tuned antennas. Light materials, such as 0.5 mm diameter copper wire, were used to tune them. These materials are not robust and they do not hold their shape with respect to the small tolerances at play. The test results showed that a difference of just 2 mm in the antenna's dimensions produce changes as large as 45 MHz in its resonant frequency. It is likely that the reduced wavelength in the dielectric phantom, which is just 15 – 20% that of free space, multiplied the impact of minor physical changes.

In the absence of reliable simulations, the empirical approach also proved effective, however repeatability was poor.

[25] Resonant frequencies ranged between 279 MHz and 473 MHz.

10. Reconciling S_{11} Predictions with Measurement Data

Section 8 described the frequency offset observed between the VNA measurements and the S_{11} frequency response predicted using the CST transient solver. This issue was not resolved at the time. It was decided to empirically refine the antenna prototypes and to revisit the simulation discrepancy at a later stage.

After the validation testing was complete, Prototype A was modelled in CST. Figure 38 shows the model with its epoxy shroud and tissue phantom hidden so that the changes to the ground plane and monopole are clearly visible.

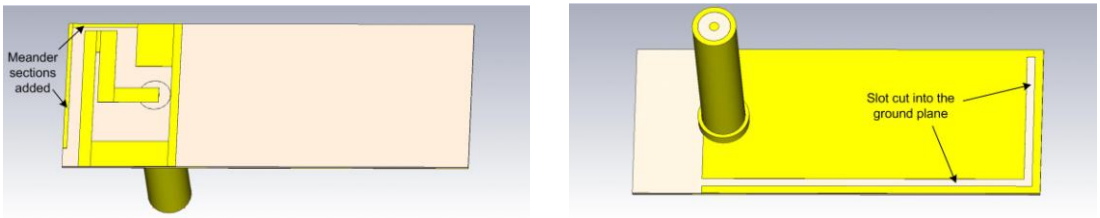

Figure 38: Prototype A was modelled in CST showing the additional meanders added to the monopole (left) and the ground plane (right).

A simulation was attempted using the CST transient solver. Again the results did not agree with the VNA measurements for Prototype A (see Figure 34 in Section 9). It was suspected that the mesh cell size may be responsible, as it is automatically optimised for the surrounding free space environment[26]. A cell size optimised for free space may be too coarse to accurately model the shorter wavelengths in a high dielectric phantom. It is recommended that the mesh cell size be at least 8 to 10 times smaller than a wavelength. The Mesh cell size was reduced but this did not improve the simulation results.

A simulation of Prototype A was then completed using the CST frequency domain solver. The S_{11} results predicted using the frequency domain solver are shown in Figure 39. The predicted resonance frequency did not agree with the VNA measurements for Prototype A. However the predicted resonance frequency (380 MHz) was a much closer fit to the measurement data than the plot predicted by the time domain solver.

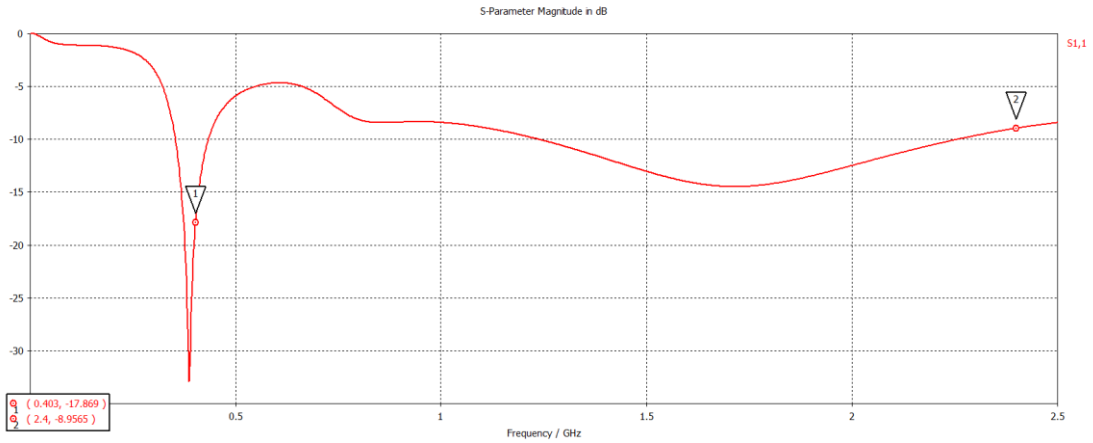

Figure 39: S_{11} prediction for Prototype A using the CST frequency domain solver.

[26] The environment at the simulation's boundary condition was free space.

11. Future Research

Monitoring of Food Spoilage through the Proxy of Antenna or Transmission Line S_{11} Characteristics

Some of the early antenna prototypes developed for this thesis were tested in phantoms that used meat samples (pork and chicken) to simulate the dielectric loading effect of body tissue. Using meat samples ultimately proved unsatisfactory as the characteristics of meat change over time. These changes influence the test antenna's frequency response and impair the repeatability of test results. The meat samples were kept sealed and refrigerated when not in use, but their characteristics were noted to change before there was visible evidence of spoiling.

If an antenna (or a terminated transmission line) is built into the food packaging it may be possible to monitor such variation and use it to characterise the onset of food spoilage. This could be applied to other food products which contain substances such as sugars that reduce[27] the dielectric constant of water, or other solvents. As these sugars are broken down by microbial activity, the resulting dielectric change may have a detectable impact on an antenna or open wire transmission line.

Much domestic food waste is avoidable. If food is stored correctly it may remain edible for a long time, but it is often discarded when it reaches the printed expiry date. Printed dates must be conservative as there is inevitable variability between samples and storage conditions may also vary. This resulting food waste[28] represents a significant annual cost to the global economy, and the UK's Waste and Resources Action Programme (WRAP) estimates the cost to be £250 to £400 per household in Britain.

Incorporating a device capable of monitoring S_{11} into disposable packaging would undoubtedly add to the cost of the food product and may also raise concerns about disposal when the packaging is discarded. However RFID is already finding its way into the packaging of many products for logistical tracking and inventory monitoring. Passive RFID tags may already incorporate many of the basic elements that would be required in order to implement an S_{11} sensing feature.

A limited review of the literature revealed some related work [28] that has been published, but it appears to be a nascent research area.

[27] This was the principle behind the liquid phantom later used in the validation testing in this thesis.
[28] 25% of all food (by weight) purchased by EU households is later discarded according to Waste and Resources Action Programme (WRAP). www.wrap.org.uk

12. References and Bibliography

[1] Dielectric Loaded Impedance Matching for Wideband Implanted Antennas: Dissanayake, Esselle and Yuce.

[2] An Ultra-low Power CMOS RF Transceiver for Medical Implants:
Bohorquez, Dawson and Chandrakasan.

[3] Electromagnetic Interactions between Biological Tissues and Implantable Biotelemetry Systems:
Kim and Rahmat-Samii.

[4] Compilation of the Dielectric Properties of Body Tissues at RF and Microwave Frequencies:
C. Gabriel and S. Gabriel.

[5] ICT implants in the human body: A review:
Fabienne Nsanze 21st December 2004

[6] Developing New Medical Implants and Diagnostic Equipment:
Hodgins, Bertsch, Post, Frischholz, Volckaerts, Spensley, Wasikiewicz, Higgins, Von Stetten and Kenney

[7] A Miniature Implanted Inverted-F Antenna for GPS Application:
Azad and Ali.

[8] Wireless Telemetry for Electronic Pill Technology:
Yuce, Dissanayake, Keong.

[9] Body Implant Communication – Is it a reality?
Henry Higgins.

[10] Body EMF Absorption: A Design Issue for Implantable Medical Electronics:
Qiang Fang.

[11] Impact of an Aortic Valve Implant on Body Surface UWB Propagation: A Preliminary Study:
Yang, Sayrafian-Pour, Hagedorn, Terrill, Yazdandoost, Taparugssanagorn, Hämäläinen and Iinatti.

[12] Wireless Power Technology for Boiomedical Implants:
Laskovsky, Dissanayake and Yuce.

[13] Mixed-Signal Integrated Circuits for Self-Contained Sub-Cubic Millimeter Biomedical Implants:
Chow, Chakraborty, Chappell and Irazoqui.

[14] Wireless Body Sensor Network using Medical Implant Band:
Yuce, Myo, Khan and Liu.

[15] Monitoring of Physiological Parameters from Multiple Patients Using Wireless Sensor Network:
Yuce, Choong and Khan.

[16] Wireless Communications Technology in Telehealth Systems:
Kailas and Ingram.

[17] A Review of Implantable Patch Antennas for Biomedical Telemetry: Challenges and Solutions:
Kiourti and Nikita.

[18] Detuning Issues and Performance of a Novel Implantable Antenna for Telemetry Applications:
Kiourti and Nikita.

[19] Radiation Characteristics of Loop Antennas for Biomedical Implants:
Abdelsayed, Nikolova and Jamal Deen.

[20] Design, Realization and Measurements of a Miniature Antenna for Implantable Wireless Communication Systems:
Merli, Bolomey, Zürcher, Corradini, Meurville and Skrivervik.

[21] The Effect of Insulating Layers on the Performance of Implanted Antennas:
Merli, Fuchs, Mosig and Skrivervik.

[22] Ultra Wideband Wireless Body Area Network for Medical Applications:
Balasingham, Chávez-Santiago, Bergsland, Ramstad and Fosse1.

[23] Design Strategies for Implantable Antennas:
Skrivervik and Merli.

[24] Radio System Design for Telecommunications. Second Edition:
Roger Freeman.

[25] Simulated biological materials for electromagnetic radiation absorption - Bioelectromagnetics, 1987" by G Hartsgrove, A Kraszewski, A Surowiec

[26] Biostability and corrosion resistance of a biocompatible encapsulation and interconnect technology for implantable electronics: Maaike Op de Beeck, Karen Qian, Karl Malachowski, Bishoy Morcos, Alex Radisic, Chris Van Hoof

[27] The Handbook of Dielectric and Thermal Properties of Materials at Microwave Frequencies: Vyacheslav V. Komarov

[28] Silk-Based Conformal, Adhesive, Edible Food Sensors: Hu Tao, Mark A. Brenckle, Miaomiao Yang, Jingdi Zhang, Mengkun Liu, Sean M. Siebert, Richard D. Averitt, Manu S. Mannoor, Michael C. McAlpine, John A. Rogers, David L. Kaplan, and Fiorenzo G. Omenetto

[29] CEPT ECC Newsletter - "Spectrum for Life; Medical Implants - A Reality for Millions" http://apps.ero.dk/eccnews/june-2011/images/ECC-Newsletter-june2011.pdf

[30] CEPT ERC Recommendation 70-03.

[31] ITU Recommendation ITU-R SA.1346.

Appendix 1 Detailed Mechanical Specifications of the Prototype Antennas

The mechanical dimensions of Prototype C are shown below. Figure 40 shows the upper side of the PCB with the monopole element and Figure 41 shows the lower ground plane side. The only design difference between Prototypes A, B and C was the length of the track on the right of Figure 40. This track was 17 mm on Prototype A, 15 mm on Prototype B and 13 mm on Prototype C. The antennas were milled on 0.4 mm thick FR4 substrate and encapsulated in a 0.15 mm layer of epoxy resin.

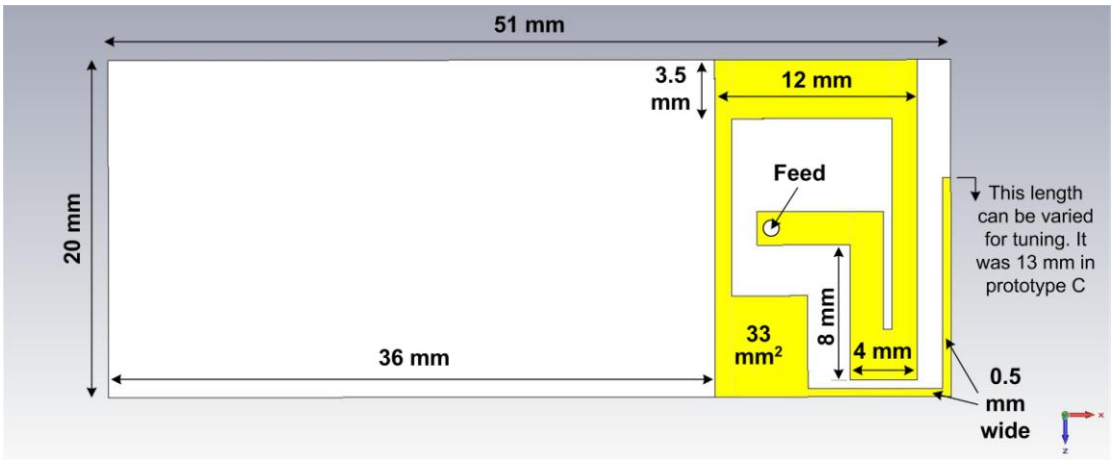

Figure 40: Monopole side of Prototypes C showing track dimensions.

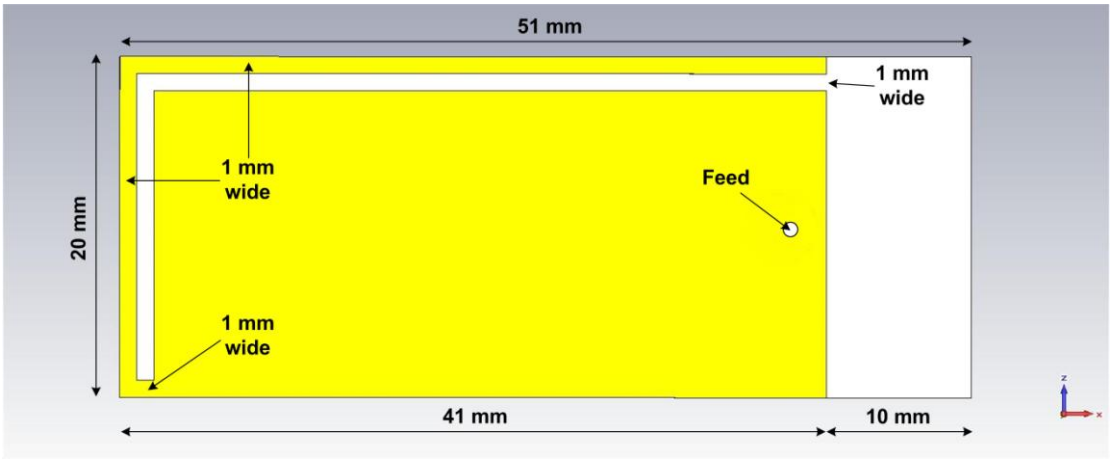

Figure 41: Ground plane side of Prototypes C showing track dimensions.

The mechanical dimensions of Prototype E are shown below. Figure 42 shows the upper side of the PCB with the monopole element and Figure 43 shows the lower ground plane side and elements of the monopole. The monopole sections were joined with a 0.5 mm diameter via. Prototype E was milled on 0.4 mm thick FR4 substrate and encapsulated in a 0.15 mm layer of epoxy resin.

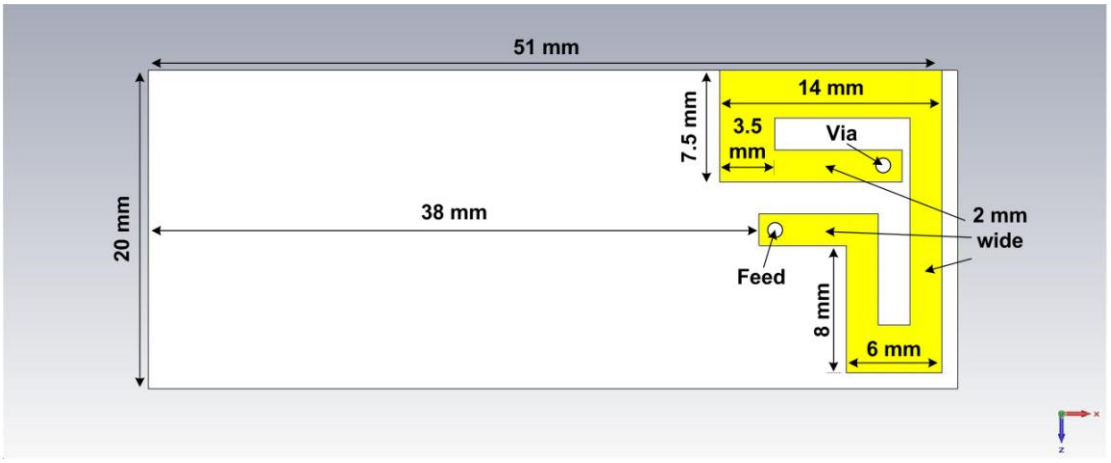

Figure 42: Monopole side of Prototype E showing track dimensions.

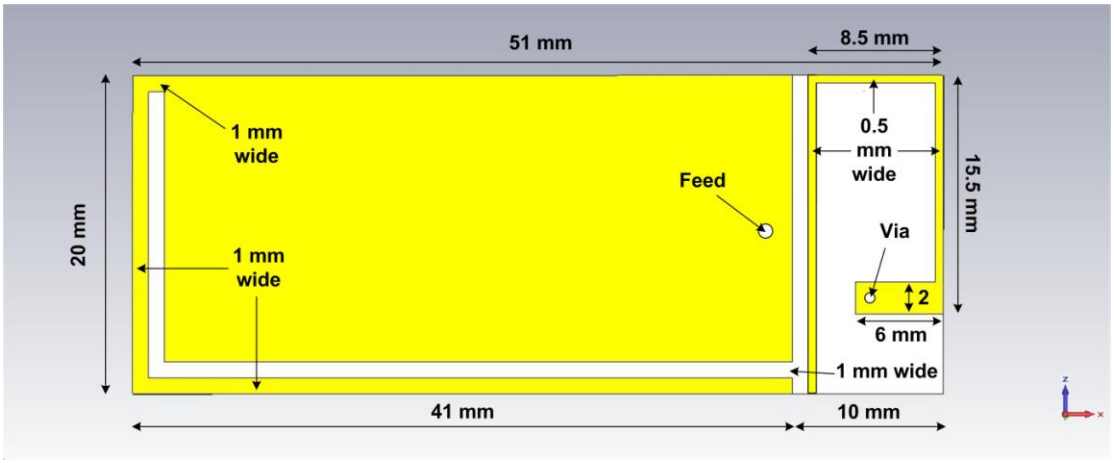

Figure 43: Monopole side of Prototype E showing track dimensions.

Appendix 2 Frequency Bands and Conditions of Use

Table 4: List of Frequency Bands and Power Levels Applicable to Active Medical Implant Devices in Europe.

Permitted Frequency Band	Permitted Power Level or Magnetic Field
402 – 405 MHz	25 µW e.r.p
401 – 402 MHz	25 µW e.r.p
405 – 406 MHz	25 µW e.r.p
9 - 315 kHz	30 dBµA/m at 10m
315 - 600 kHz	-5 dBµA/m at 10m
30.0 - 37.5 MHz	1 mW e.r.p.
12.5 - 20.0 MHz	-7 dBµA/m at 10m
2483.5 - 2500 MHz	10 dBm e.i.r.p

Source: ERC Recommendation 70-03:
http://www.erodocdb.dk/docs/doc98/official/pdf/rec7003e.pdf

Table 5: List of Frequency Bands and Power Levels Applicable to Non-specific Short Range Devices in Europe.

Permitted Frequency Band	Permitted Power Level or Magnetic Field
6765 - 6795 kHz	42 dBµA/m at 10m
13.553 - 13.567 MHz	42 dBµA/m at 10m
26.957 - 27.283 MHz	42 dBµA/m at 10m 10 mW e.r.p
40.660 - 40.700 MHz	10 mW e.r.p.
138.20 - 138.45 MHz	10 mW e.r.p.
433.050 - 434.790 MHz	10 mW e.r.p.
433.050 - 434.790 MHz	1 mW e.r.p. -13 dBm/10 kHz
434.040 - 434.790 MHz	10 mW e.r.p.
863 - 870 MHz	≤ 25 mW e.r.p. (DSSS with LBT and AFA)
2400.0 - 2483.5 MHz	10 mW e.i.r.p.
5725 - 5875 MHz	25 mW e.i.r.p.
24.00 - 24.25 GHz	100 mW e.i.r.p.
61.0 - 61.5 GHz	100 mW e.i.r.p.
57 - 64 GHz	100 mW e.i.r.p.
122 - 123 GHz	100 mW e.i.r.p.
244 - 246 GHz	100 mW e.i.r.p.

Note on Tables 4 and 5. Please note that additional mitigation requirements apply to many of the bands listed above. These requirements include limitations on duty cycle and implementation of techniques such as listen before talk (LBT) and Adaptive Frequency Agility (AFA). For further details please see Annex 1 and 12 of ERC Rec 70-03.

Source: ERC Recommendation 70-03:
http://www.erodocdb.dk/docs/doc98/official/pdf/rec7003e.pdf

Table 6: List of Frequency Bands and Permitted Channel Bandwidths Applicable to Active Medical Implant Devices in the United States.

Permitted Frequency Band	Permitted Bandwidth
401 - 401.85 MHz	100 kHz
401.85 - 402 MHz	150 kHz
402 - 405 MHz	300 kHz
405 - 406 MHz	100 kHz
413 - 419 MHz	6 MHz
426 - 432 MHz	6 MHz
438 - 444 MHz	6 MHz
451 - 457 MHz	6 MHz

Source:
http://www.fcc.gov/encyclopedia/medical-device-radiocommunications-service-medradio

Table 7: List of frequency bands identified for use by Industrial, Scientific and Medical Applications in the United States.

Permitted Frequency Band
6.765 - 6.795 MHz
13.553 - 13.567 MHz
26.957 - 27.283 MHz
40.660 - 40.700 MHz
433.050 - 434.790 MHz
902.000 - 928.000 MHz
2400 - 2500 MHz
5.725 - 5.875 GHz
24.000 - 24.250 GHz
61.000 - 61.500 GHz
122.000 - 123.000 GHz
244.000 - 246.000 GHz

Source:
http://www.gpo.gov/fdsys/pkg/CFR-2007-title47-vol1/pdf/CFR-2007-title47-vol1-part18.pdf

Appendix 3 Simulation Results - Analysis of the Observed Discrepancy Between the Predictions and Measurement Data.

Investigation 1 - The impact of variations in the phantom material and its effect on antenna resonant frequency.

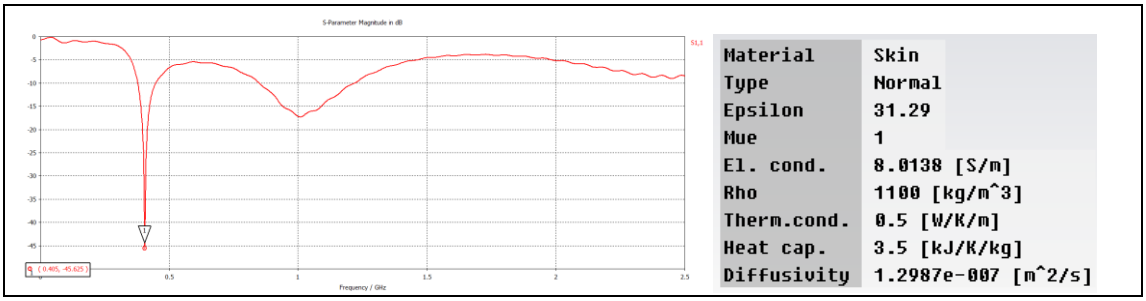

Figure 44: Skin tissue phantom with 2 mm thick glycerine shroud with resonance at 405 MHz.

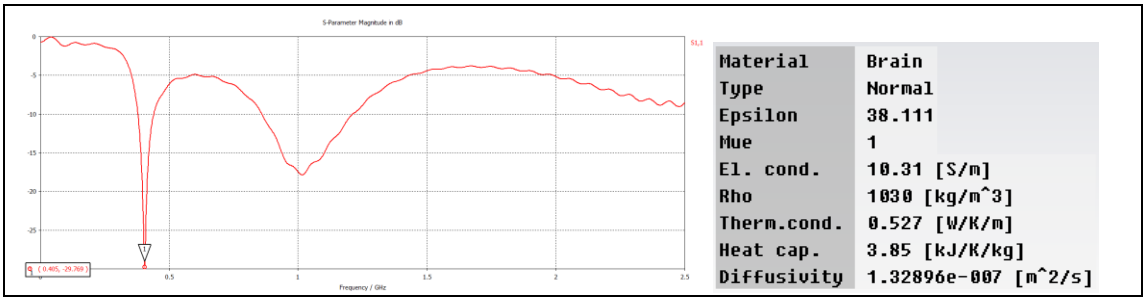

Figure 45: Brain tissue phantom with 2 mm thick glycerine shroud: Resonance at 405 MHz.

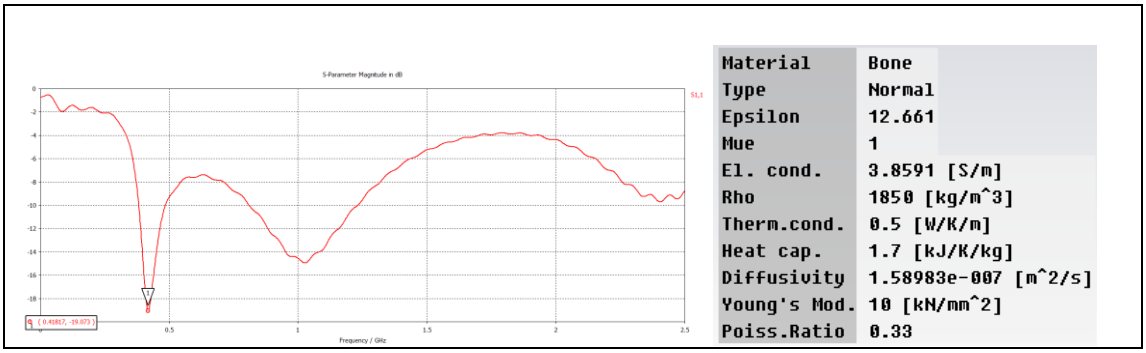

Figure 46: Bone tissue phantom with 2 mm thick glycerine shroud: Resonance at 418 MHz.

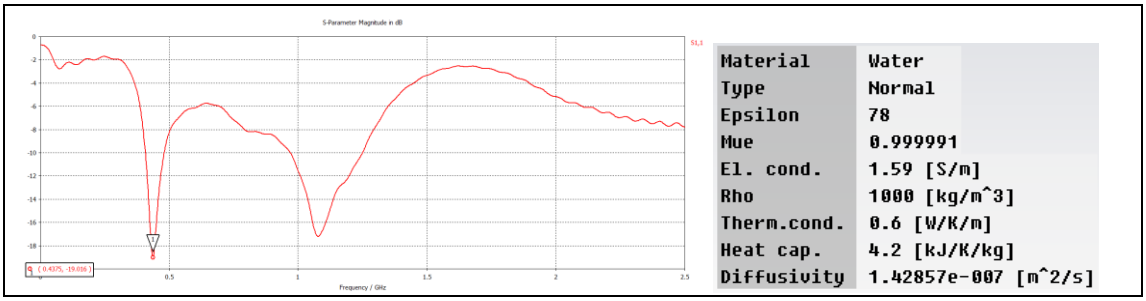

Figure 47: Tap water phantom with 2 mm thick glycerine shroud: Resonance at 437 MHz.

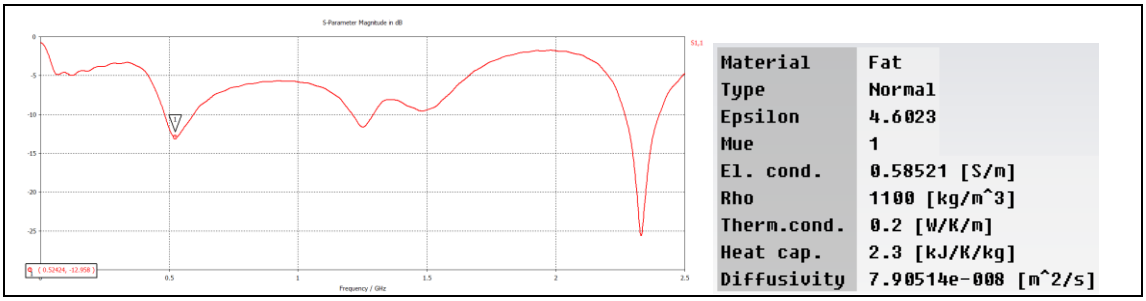

Figure 48: Fat tissue phantom with 2 mm thick glycerine shroud: Resonance at 524 MHz.

Table 1 from Section 8 is shown here again for ease of comparison with diagrams.

Phantom material	Dielectric constant (Epsilon)	Magnetic permeability (Mue)	Electrical conductivity	Antenna resonance frequency	**Deviation from 405 MHz**
Skin	31.29	1	8.0138 S/m	405 MHz	**0 MHz**
Brain	38.111	1	10.31 S/m	405 MHz	**0 MHz**
Bone	12.66	1	3.8591 S/m	418 MHz	**+ 13 MHz**
Tap Water	78	0.999991	1.59 S/m	437 MHz	**+ 32 MHz**
Fat	4.6	1	0.58521 S/m	524 MHz	**+ 119 MHz**

Table 1: Effect of various phantom materials of antenna resonant frequency.

Investigation 2 - The effects of common mode on the coaxial feeder.

The V49 antenna model was simulated[29] with two different lengths of coaxial feeder (4 mm and 125 mm). In both cases S_{11} was maximum at 406 MHz, see the below plots. It is evident from the results that common mode current on the feeder does not effect the resonance frequency in the CST simulations. The 5 dB S_{11} difference between the plots is the result of feeder loss in the additional 121 mm of coaxial feeder.

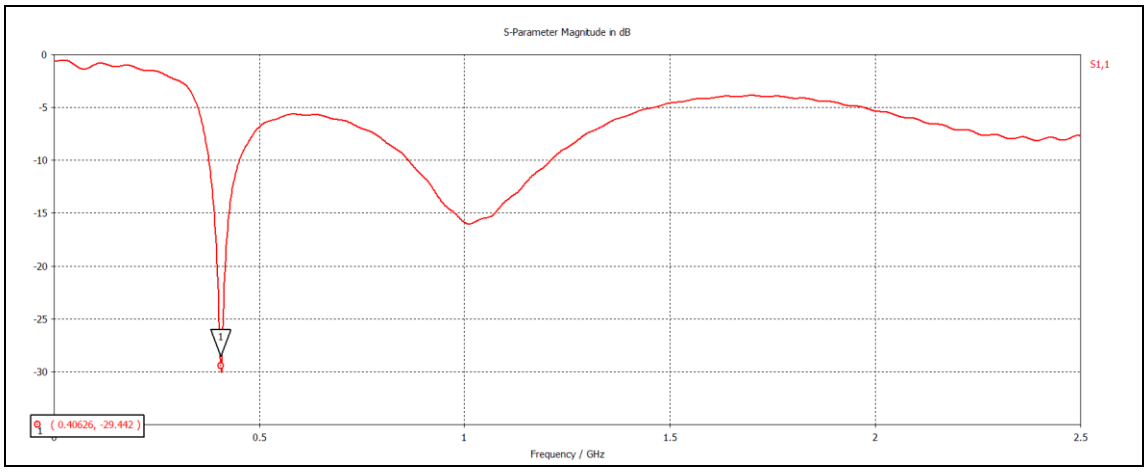

Figure 49: The resonance frequency is 406 MHz with **4 mm** of coaxial feeder.

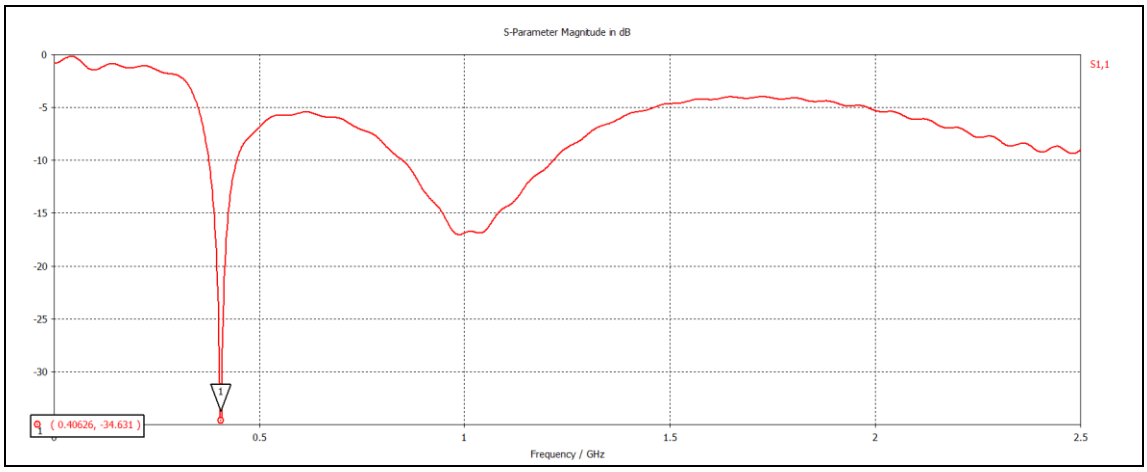

Figure 50: The resonance frequency is 406 MHz with **125 mm** of coaxial feeder.

[29] The simulations used the CST the transient solver.

Investigation 3 - Agreement between free space S_{11} predictions and measurements.

The frequency discrepancy was observed between the predictions and measurements when both were in a dielectrically loaded condition. The S_{11} performance was simulated and measured in the un-loaded condition (i.e. without a phantom) for comparison purposes. The prediction and measurement data agreed closely, indicating that the discrepancy is related to the effects of dielectric loading. The measurements showed a 2 dB increase in S_{11} at higher frequencies (circa 2.5 GHz). This is again due to the lower feeder losses in the CST model.

Investigation into the need for a glycerine shroud

In order to determine if a glycerine shroud was necessary, two simulations were run with and without a glycerine shroud.

Figure 51 shows the radiation pattern and loss with a 2 mm thick glycerine layer between the antenna and the phantom. Figure 52 presents the same information for a 2 mm void between the antenna and phantom.

Removing the shroud creates nulls normal to the plan of the substrate. However, the overall radiation pattern is not significantly perturbed when the shroud is removed, with in directivity differing by less than 0.5 dB).

The most surprising effect of removing glycerine is in radiation efficiency. There was 43 dB of loss when the glycerine shroud was included. When it is removed the loss is reduced to 41 dB. This defeats the purpose of using glycerine, as the reason for including it is to increase radiation efficiency by matching the antenna to the dielectric of the phantom. It appears from the results of these simulations and the prototype tests, that the inclusion of glycerine has a negative impact on antenna performance.

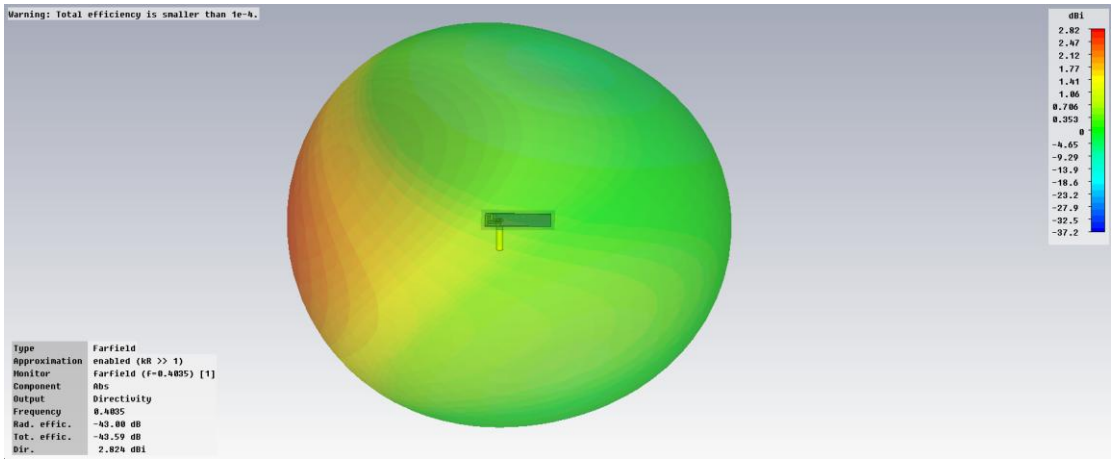

Figure 51: Radiation pattern of prototype in phantom with a 2 mm glycerine shroud.

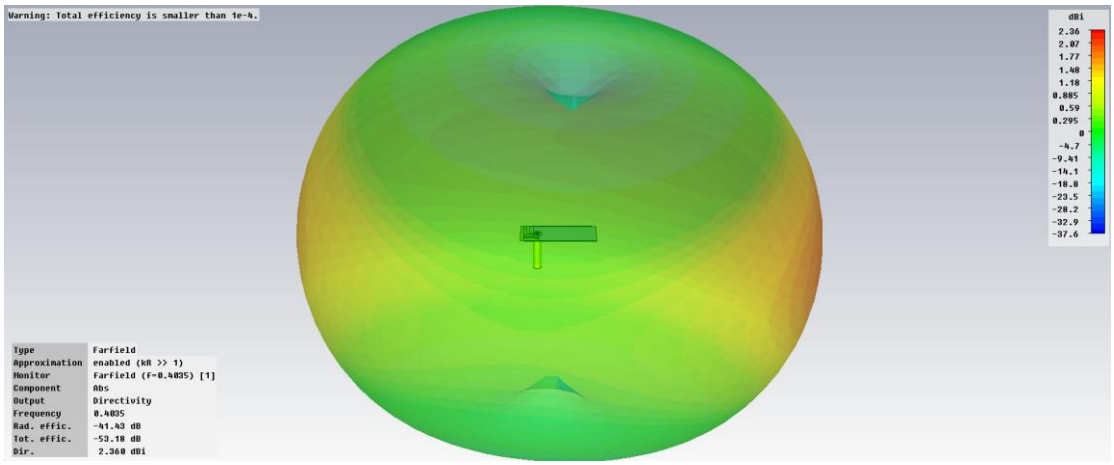

Figure 52: Radiation pattern of prototype in phantom without a shroud (2 mm void between antenna elements and phantom).

Appendix 4 Validation Data - Tabular S_{11} Values

Table 8

Frequency (MHz)	Prototype A (dB)	Prototype B (dB)	Prototype C (dB)	Prototype E (dB)
10	-12.6	-11.1	-8.4	-3.4
25	-10.9	-10.7	-8.7	-5.1
40	-9.5	-9.2	-8.3	-5.9
55	-8.4	-8.2	-7.5	-6.0
70	-7.8	-7.5	-6.8	-5.8
85	-7.3	-7.0	-6.3	-5.6
100	-7.0	-6.8	-6.0	-5.6
115	-6.9	-6.6	-5.8	-5.5
130	-6.7	-6.4	-5.5	-5.4
145	-6.5	-6.2	-5.3	-5.1
160	-6.5	-6.2	-5.1	-5.0
174	-6.7	-6.3	-5.0	-4.8
189	-7.1	-6.6	-5.1	-4.9
204	-7.6	-7.1	-5.3	-5.2
219	-8.3	-7.7	-5.6	-5.4
234	-8.8	-8.3	-6.0	-5.6
249	-9.2	-8.9	-6.3	-5.5
264	-9.4	-9.5	-6.9	-5.6
279	-9.5	-10.1	-7.9	-5.7
294	-9.4	-10.5	-9.2	-6.1
309	-9.3	-10.6	-11.0	-6.8
324	-9.0	-10.5	-12.9	-7.8
339	-8.7	-10.0	-14.3	-9.0
354	-8.2	-9.4	-14.5	-10.5
369	-7.7	-8.6	-13.5	-12.6
384	-7.1	-8.0	-12.1	-15.6
399	-6.8	-7.5	-10.8	-19.3
414	-6.6	-7.2	-9.8	-22.4
429	-6.5	-7.0	-9.1	-24.7
444	-6.4	-6.9	-8.6	-27.9
459	-6.4	-6.9	-8.2	-34.2
473	-6.2	-6.7	-7.6	-37.2
488	-6.1	-6.6	-7.1	-26.8
503	-6.0	-6.5	-6.7	-20.5
518	-6.1	-6.6	-6.4	-16.7
533	-6.4	-6.9	-6.2	-14.1
548	-6.8	-7.3	-6.2	-12.4
563	-7.2	-7.7	-6.3	-11.4
578	-7.7	-8.2	-6.3	-10.6
593	-8.0	-8.5	-6.3	-9.9
608	-8.4	-8.9	-6.3	-9.2
623	-8.9	-9.4	-6.4	-8.5
638	-9.4	-10.0	-6.5	-7.9
653	-10.1	-10.7	-6.8	-7.6
668	-10.8	-11.4	-7.2	-7.3
683	-11.3	-11.9	-7.5	-7.2
698	-11.5	-12.1	-7.9	-7.1
713	-11.5	-12.0	-8.1	-6.9
728	-11.3	-11.8	-8.4	-6.6
743	-11.1	-11.6	-8.8	-6.4
758	-10.9	-11.4	-9.2	-6.2
772	-10.8	-11.4	-9.8	-6.2
787	-10.7	-11.3	-10.4	-6.2
802	-10.6	-11.2	-10.8	-6.2
817	-10.4	-10.9	-11.1	-6.1
832	-10.1	-10.5	-11.3	-6.0
847	-9.7	-10.1	-11.3	-5.8
862	-9.4	-9.8	-11.2	-5.7
877	-9.2	-9.5	-11.2	-5.6
892	-9.1	-9.3	-11.2	-5.6
907	-9.1	-9.2	-11.2	-5.6
922	-9.0	-9.1	-11.2	-5.6
937	-9.0	-9.0	-11.0	-5.5
952	-8.9	-8.8	-10.8	-5.5
967	-8.8	-8.7	-10.6	-5.5
982	-8.8	-8.6	-10.5	-5.5
997	-8.8	-8.6	-10.4	-5.6
1012	-8.9	-8.6	-10.4	-5.7
1027	-9.0	-8.6	-10.4	-5.8
1042	-9.1	-8.6	-10.4	-5.9
1057	-9.2	-8.6	-10.4	-6.1
1071	-9.2	-8.5	-10.4	-6.2
1086	-9.2	-8.5	-10.3	-6.5
1101	-9.3	-8.5	-10.3	-6.8
1116	-9.4	-8.5	-10.3	-7.2
1131	-9.5	-8.6	-10.5	-7.7
1146	-9.7	-8.8	-10.7	-8.4
1161	-9.8	-8.9	-10.8	-9.0
1176	-10.0	-9.0	-11.1	-9.8
1191	-10.2	-9.1	-11.2	-10.7
1206	-10.3	-9.2	-11.3	-11.6
1221	-10.3	-9.2	-11.3	-12.6
1236	-10.3	-9.2	-11.3	-13.7
1251	-10.3	-9.2	-11.3	-15.0
1266	-10.3	-9.2	-11.4	-16.4
1281	-10.3	-9.3	-11.4	-17.7
1296	-10.4	-9.4	-11.5	-18.7
1311	-10.4	-9.5	-11.6	-19.0
1326	-10.5	-9.6	-11.7	-18.7
1341	-10.4	-9.6	-11.7	-17.8
1356	-10.3	-9.6	-11.7	-16.8
1370	-10.2	-9.6	-11.6	-15.7
1385	-10.1	-9.7	-11.6	-14.8
1400	-10.1	-9.8	-11.6	-14.1
1415	-10.1	-9.9	-11.7	-13.5
1430	-10.1	-9.9	-11.7	-13.0
1445	-10.0	-9.9	-11.7	-12.4
1460	-9.8	-9.8	-11.5	-11.9
1475	-9.6	-9.7	-11.3	-11.3
1490	-9.4	-9.6	-11.1	-10.8
1505	-9.2	-9.6	-11.0	-10.4
1520	-9.1	-9.6	-11.0	-10.3

1535	-9.1	-9.6	-11.0	-10.2
1550	-9.0	-9.7	-11.1	-10.2
1565	-8.9	-9.6	-11.0	-10.1
1580	-8.7	-9.4	-10.8	-9.9
1595	-8.5	-9.1	-10.5	-9.7
1610	-8.2	-8.9	-10.3	-9.6
1625	-8.1	-8.8	-10.1	-9.7
1640	-8.0	-8.8	-10.0	-9.8
1655	-8.0	-8.8	-10.1	-10.0
1669	-8.0	-8.7	-10.1	-10.2
1684	-7.9	-8.6	-10.0	-10.2
1699	-7.7	-8.3	-9.8	-10.1
1714	-7.5	-8.0	-9.4	-9.9
1729	-7.3	-7.8	-9.1	-9.8
1744	-7.2	-7.7	-8.9	-9.8
1759	-7.2	-7.7	-8.9	-9.9
1774	-7.2	-7.7	-8.9	-10.0
1789	-7.3	-7.6	-8.9	-10.0
1804	-7.2	-7.5	-8.8	-9.9
1819	-7.0	-7.2	-8.6	-9.6
1834	-6.9	-7.0	-8.3	-9.3
1849	-6.7	-6.9	-8.1	-9.0
1864	-6.7	-6.9	-7.9	-8.9
1879	-6.8	-6.9	-8.0	-8.9
1894	-6.9	-7.0	-8.0	-8.9
1909	-6.9	-6.9	-8.0	-8.8
1924	-6.8	-6.8	-7.9	-8.5
1939	-6.7	-6.5	-7.7	-8.2
1954	-6.5	-6.4	-7.4	-7.8
1968	-6.5	-6.3	-7.3	-7.6
1983	-6.5	-6.3	-7.2	-7.5
1998	-6.6	-6.4	-7.2	-7.5
2013	-6.6	-6.5	-7.3	-7.5
2028	-6.7	-6.4	-7.3	-7.4
2043	-6.6	-6.3	-7.2	-7.2
2058	-6.5	-6.2	-7.0	-7.0
2073	-6.4	-6.1	-6.8	-6.8
2088	-6.4	-6.1	-6.8	-6.7
2103	-6.5	-6.2	-6.8	-6.7
2118	-6.6	-6.3	-6.9	-6.8
2133	-6.7	-6.4	-6.9	-6.8
2148	-6.7	-6.3	-7.0	-6.7
2163	-6.6	-6.2	-6.9	-6.6
2178	-6.6	-6.1	-6.8	-6.5
2193	-6.5	-6.1	-6.7	-6.4
2208	-6.5	-6.2	-6.7	-6.4
2223	-6.6	-6.3	-6.7	-6.5
2238	-6.7	-6.3	-6.8	-6.5
2253	-6.8	-6.3	-6.9	-6.5
2267	-6.8	-6.3	-6.9	-6.5
2282	-6.7	-6.2	-6.8	-6.4
2297	-6.7	-6.2	-6.7	-6.3
2312	-6.7	-6.2	-6.7	-6.3
2327	-6.7	-6.2	-6.7	-6.3
2342	-6.8	-6.2	-6.8	-6.4
2357	-6.8	-6.3	-6.8	-6.4
2372	-6.8	-6.2	-6.8	-6.4
2387	-6.7	-6.1	-6.8	-6.3
2402	-6.7	-6.1	-6.7	-6.2
2417	-6.6	-6.0	-6.6	-6.2
2432	-6.6	-6.1	-6.6	-6.2
2447	-6.6	-6.1	-6.6	-6.3
2462	-6.7	-6.1	-6.7	-6.3
2477	-6.7	-6.1	-6.7	-6.3
2492	-6.7	-6.1	-6.7	-6.3
2507	-6.7	-6.1	-6.7	-6.3
2522	-6.6	-6.0	-6.6	-6.2
2537	-6.6	-6.0	-6.5	-6.2
2552	-6.6	-6.0	-6.5	-6.2
2566	-6.6	-6.0	-6.5	-6.2
2581	-6.6	-6.0	-6.5	-6.2
2596	-6.5	-5.9	-6.5	-6.2
2611	-6.5	-5.9	-6.4	-6.2
2626	-6.5	-5.9	-6.4	-6.2
2641	-6.5	-5.9	-6.4	-6.2
2656	-6.5	-6.0	-6.4	-6.3
2671	-6.5	-6.0	-6.4	-6.3
2686	-6.6	-6.0	-6.5	-6.3
2701	-6.6	-6.0	-6.5	-6.3
2716	-6.5	-6.0	-6.4	-6.3
2731	-6.5	-5.9	-6.4	-6.3
2746	-6.5	-6.0	-6.4	-6.3
2761	-6.5	-6.0	-6.4	-6.4
2776	-6.6	-6.0	-6.5	-6.4
2791	-6.6	-6.1	-6.5	-6.5
2806	-6.6	-6.1	-6.6	-6.5
2821	-6.6	-6.1	-6.6	-6.5
2836	-6.6	-6.1	-6.6	-6.5
2851	-6.6	-6.1	-6.6	-6.5
2865	-6.6	-6.1	-6.6	-6.6
2880	-6.7	-6.2	-6.7	-6.7
2895	-6.7	-6.2	-6.8	-6.7
2910	-6.8	-6.2	-6.8	-6.7
2925	-6.7	-6.1	-6.8	-6.7
2940	-6.7	-6.1	-6.8	-6.6
2955	-6.6	-6.1	-6.7	-6.6
2970	-6.6	-6.1	-6.7	-6.6
2985	-6.6	-6.1	-6.7	-6.7
3000	-6.7	-6.2	-6.8	-6.7

Appendix 5 Coplanar Waveguide Feeders

The antenna shown below in Figure 53 was designed in CST and its performance was simulated from 350 MHz to 1500 MHz for two different scenarios; a free space environment and a skin tissue phantom. The dimensions of the antenna model were 50 mm x 20 mm. It consisted of 35 µm annealed copper on a 400 µm thick FR4 (lossy) substrate. The port arrangement consisted of a waveguide port coupled into a Teflon dielectric coax with conductor and dielectric dimensions similar to an SMA connector. This in turn coupled to a CPW transmission line with tracks spaced for line 50 Ω characteristic impedance, which fed a meandered inverted-L antenna.

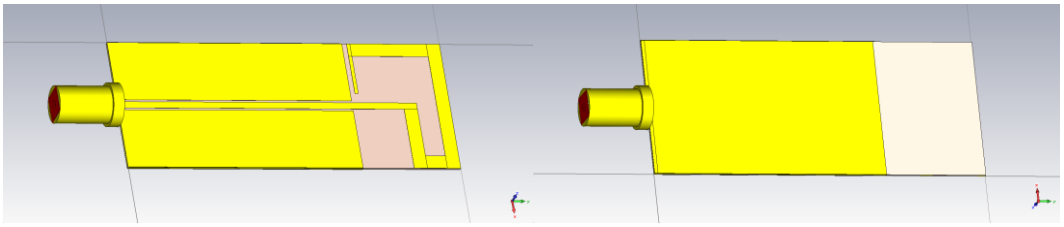

Figure 53: Antenna model with a CPW feeder, showing the upper monopole and CPW side (left) and the lower ground plane side (right).

CST modelling in free space

Figure 54 show the CST predictions for S_{11} in free space (i.e. with no dielectric loading other than that of the FR4 substrate material). The marker points in each plot indicate the antenna's S_{11} performance at 403 MHz. The return loss in free space reached a maximum of 11 dB at 1268 MHz. The frequency range of the simulation was 350 MHz to 1500 MHz.

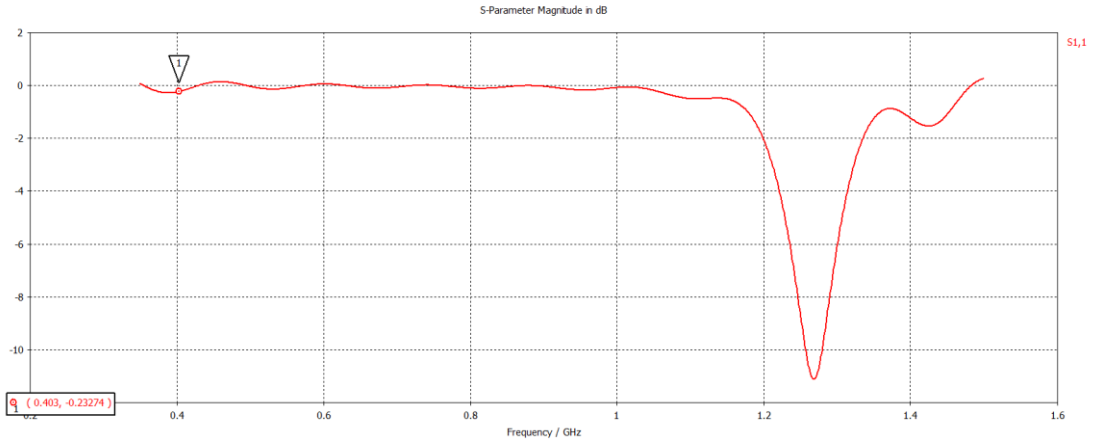

Figure 54: Scalar prediction of S_{11} for the unloaded free space antenna model.

CST Modelling in phantom

Figure 55 show the CST antenna model adapted for an *in vivo* simulation by adding a surrounding glycerine shroud and tissue phantom. The antenna's performance was simulated over the range 350 MHz to 1500 MHz and the results are presented in Figure 56. The dielectric loading associated with the glycerine and tissue phantom lowers the resonance frequency to 430 MHz (from 1268 MHz in free space). CST predicts a S_{11} value of 9.5 dB at 403 MHz, reaching a maximum of 21 dB at 430 MHz.

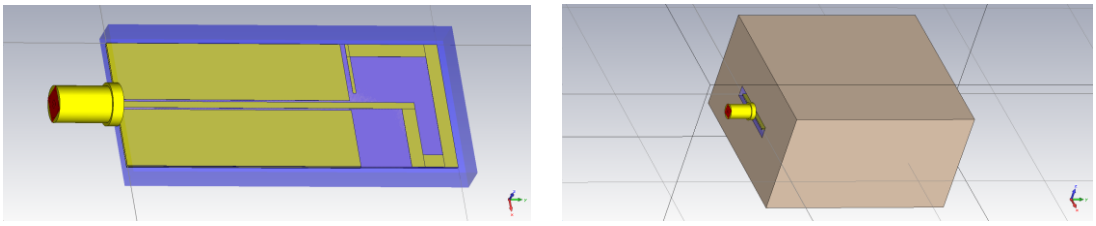

Figure 55: The CST antenna model with a surrounding 2 mm inner layer of glycerine (left) and immersed in a 20 mm outer layer of tissue phantom (right).

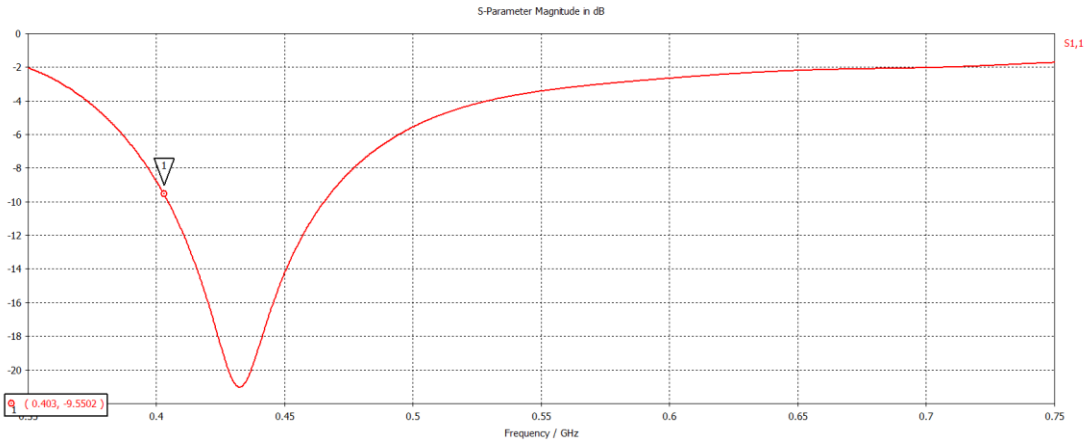

Figure 56: Scalar prediction of S_{11} for the dielectrically loaded antenna in the phantom.

Developing a Prototype Antenna

A crude prototype antenna was produced using copper EMC screening tape and a 1.6mm thick PCB substrate of unknown dielectric constant. The dimensions of the prototype antenna were 50 mm x 20 mm, not including the SMA connector. Figure 57 shows the upper and lower faces of the prototype. The ground planes of the two faces are soldered along the edges of the substrate.

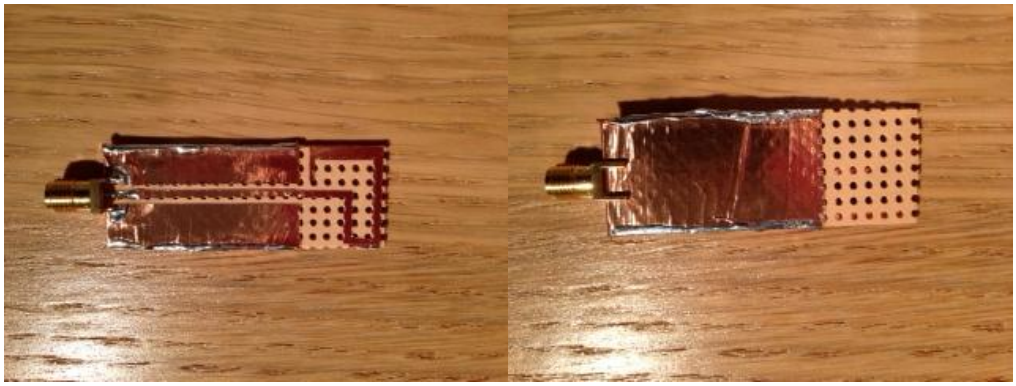

Figure 57: The upper and lower surfaces of an early monopole with CPW feeder.

The measurement used a tissue phantom consisting of raw chicken breast mussel. The tissue was incised and the incision was lined with a thin layer of polythene film. The void was filled with 5 ml of liquid glycerine.

The prototype antenna was immersed in the pool of glycerine and S_{11} was measured using a VNA. At 403 MHz the return loss was 12 dB with 36.8 Ω real resistance and 18 Ω of inductive reactance. S_{11} peaked at 470 MHz with a return loss of 18 dB.

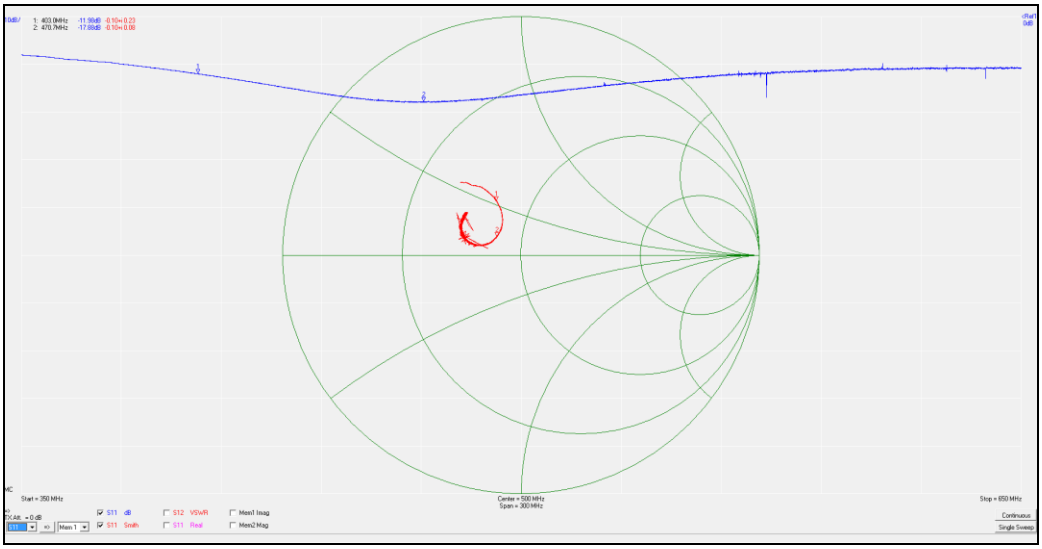

Figure 58: S_{11} measurement with the CPW feed antenna under dielectrically loaded conditions.